# REPORT DOCUMENTATION PAGE

*Form Approved*
*OMB No. 0704-0188*



| **1. REPORT DATE** *(DD-MM-YYYY)* | **2. REPORT TYPE** | **3. DATES COVERED** *(From - To)* |
|---|---|---|
| 14-10-2020 | Interim Journal Article | 01 Oct 2019 – 1 Oct 2020 |

**4. TITLE AND SUBTITLE**
Computational Modeling and Damage Threshold Prediction of Continuous-Wave and Multiple-Pulse Porcine Skin Laser Exposures at 1070 nm

**5a. CONTRACT NUMBER**
FA8650-19-C-6024

**5b. GRANT NUMBER**

**5c. PROGRAM ELEMENT NUMBER**

**6. AUTHOR(S)**
Michael P. DeLisi, Nicholas J. Gamez, Clifton D. Clark III, Semih S. Kumru, Benjamin A. Rockwell, Robert J. Thomas

**5d. PROJECT NUMBER**

**5e. TASK NUMBER**

**5f. WORK UNIT NUMBER**
H0NU

**7. PERFORMING ORGANIZATION NAME(S) AND ADDRESS(ES)**
SAIC, Inc
4141 Petroleum Rd
JBSA Fort Sam Houston TX
78234-2644

**8. PERFORMING ORGANIZATION REPORT NUMBER**

**9. SPONSORING / MONITORING AGENCY NAME(S) AND ADDRESS(ES)**
Air Force Research Laboratory
711th Human Performance Wing
Airman Systems Directorate
Bioeffects Division
Optical Radiation Bioeffects Branch
4141 Petroleum Rd
JBSA Fort Sam Houston TX 78234-2644

**10. SPONSOR/MONITOR'S ACRONYM(S)**

**11. SPONSOR/MONITOR'S REPORT NUMBER(S)**
AFRL-RH-FS-JA-2021-0002

**12. DISTRIBUTION / AVAILABILITY STATEMENT**
Distribution Statement A. Approved for public release; distribution is unlimited. PA Case #: TSRL-PA-20-0200. The opinions expressed on this document, electronic or otherwise, are solely those of the author(s). They do not represent an endorsement by or the views of the United States Air Force, the Department of Defense, or the United States Government.

**13. SUPPLEMENTARY NOTES**

**14. Abstract**
Computational models are capable of simulating the expected thermal response of biological tissue to laser irradiation. A typical laser-tissue model accounts for optical energy deposition, heat transfer, and damage assessment, with the latter often represented by calculation of the Arrhenius integral. Previous studies have successfully employed these methods to predict skin damage thresholds at laser wavelengths with high absorption in water, and usually for single continuous-wave exposures. However, there remains a need for a robust and accurate predictive model in low-absorption, high-scattering cases, such as for exposures in the near-infrared region near 1000 nm. This study presents a framework for modeling laser irradiation of skin tissue at 1070-nm for both continuous-wave and pulsed exposures with durations ranging from $10^{-2}$ to $10^{1}$ seconds. We derive an optical absorption coefficient for the epidermis that agrees with expected chromophore distribution and report the modeled skin thermal responses alongside surface thermography data from *in vivo* porcine exposures as validation of simulation accuracy. Comparisons of modeled damage thresholds calculated by the Arrhenius integral with documented experimentally-determined minimum visible lesion $ED_{50}$ data exhibit a high degree of agreement.

**15. SUBJECT TERMS**
Laser damage threshold, mnimum visible, laser skin injury, near-infrared lasers, laser skin model, thermal model, Arrhenius integral

| **16. SECURITY CLASSIFICATION OF:** | | | **17. LIMITATION OF ABSTRACT** | **18. NUMBER OF PAGES** | **19a. NAME OF RESPONSIBLE PERSON** |
|---|---|---|---|---|---|
| **a. REPORT** | **b. ABSTRACT** | **c. THIS PAGE** | | | Dr. Semih Kumru |
| U | U | U | SAR<br>Unclassified | 28 | **19b. TELEPHONE NUMBER** *(include area code)*<br>210-539-8244 |

Journal of Laser Applications

# Computational modeling and damage threshold prediction of continuous-wave and multiple-pulse porcine skin laser exposures at 1070 nm

Cite as: J. Laser Appl. 33, 022023 (2021); https://doi.org/10.2351/7.0000367
Submitted: 27 January 2021 . Accepted: 21 April 2021 . Published Online: 11 May 2021

Michael P. DeLisi, Nicholas J. Gamez, Clifton D. Clark, Semih S. Kumru, Benjamin A. Rockwell, and Robert J. Thomas

Journal of Laser Applications ARTICLE scitation.org/journal/jla

# Computational modeling and damage threshold prediction of continuous-wave and multiple-pulse porcine skin laser exposures at 1070 nm

Cite as: J. Laser Appl. 33, 022023 (2021); doi: 10.2351/7.0000367
Submitted: 27 January 2021 · Accepted: 21 April 2021 ·
Published Online: 11 May 2021



Michael P. DeLisi,[1,a)] Nicholas J. Gamez,[1] Clifton D. Clark, III,[1,2] Semih S. Kumru,[3] Benjamin A. Rockwell,[3] and Robert J. Thomas[3]

## AFFILIATIONS

[1]SAIC, JBSA Fort Sam Houston, Texas 78234
[2]Department of Physics, Fort Hays State University, Hays, Kansas 67601
[3]711th Human Performance Wing, Airman Systems Directorate, Bioeffects Division, JBSA Fort Sam Houston, Texas 78234

[a)]**Author to whom correspondence should be addressed; electronic mail:** michael.p.delisi@saic.com

## ABSTRACT

Computational models are capable of simulating the expected thermal response of biological tissue to laser irradiation. A typical laser tissue model accounts for optical energy deposition, heat transfer, and damage assessment, with the latter often represented by calculation of the Arrhenius integral. Previous studies have successfully employed these methods to predict skin damage thresholds at laser wavelengths with high absorption in water, and usually for single continuous-wave exposures. However, there remains a need for a robust and accurate predictive model in low-absorption, high-scattering cases, such as for exposures in the near-infrared region near 1000 nm. This study presents a framework for modeling laser irradiation of skin tissue at 1070 nm for both continuous-wave and pulsed exposures with durations ranging from $10^{-2}$ to $10^{1}$ s. The authors derive an optical absorption coefficient for the epidermis that agrees with expected chromophore distribution and report the modeled skin thermal responses alongside surface thermography data from *in vivo* porcine exposures as validation of simulation accuracy. Comparisons of modeled damage thresholds calculated by the Arrhenius integral with documented experimentally determined minimum visible lesion $ED_{50}$ data exhibit a high degree of agreement. The authors also provide new Arrhenius rate process coefficients of $A = 2.74 \times 10^{94}\ s^{-1}$ and $E_a = 5.90 \times 10^{5}$ J/mol, determined from experimental thermal profiles with a unique method, that demonstrate more accurate threshold predictions than those used in previous modeling studies. The techniques outlined by this study provide a useful tool in assessing potentially hazardous near-infrared laser exposure scenarios.

Key words: laser damage threshold, minimum visible lesion, laser skin injury, near-infrared lasers, laser skin model, thermal model, Arrhenius integral, rate process coefficients



## I. INTRODUCTION

Knowledge of laser-induced tissue damage thresholds is vital to the field of laser safety, particularly in the skin and eye, where they inform establishment of the maximum permissible exposure (MPE) limits in the ANSI Z136.1 standard.[1] In the context of skin exposure, the near-infrared (NIR) wavelength region (750–1400 nm) has often been considered among the least hazardous,[2] as it features low absorption in the tissue. However, the region near 1000 nm has become increasingly relevant to laser safety in recent years due to the proliferation of diode-pumped fiber lasers and other high-energy systems that are capable of depositing large amounts of energy in a concentrated area over small windows of time.

Laser injury thresholds are typically expressed as the necessary laser energy required to produce a minimum visible lesion (MVL), usually manifesting as minimally visible erythema or reddening of

the skin, as judged by a set of experienced observers. MVL thresholds are often reported as the effective dose required for a 50% probability of observing the effect in question, known as the $ED_{50}$, and calculated with the probit method.[3] Experimental determination of MVL thresholds is a very broad area of study even when limited to skin tissue, depending on tissue chromophore distribution (such as pigment and water), laser wavelength, pulse duration, and exposure parameters that may influence the tissue damage mechanism.

Hazard assessments of laser interaction with skin near 1000 nm are based on a few past experimental studies. Rockwell and Goldman conducted one of the first comprehensive studies of laser skin damage, which included determination of MVL thresholds for 75 ns and 1 s exposures at 1060 nm for low- and high-pigmented human skin.[4] Most recent studies have utilized porcine skin as a substitute for human skin, particularly the Yucatan mini-pig breed, which features similar physiological properties, pigment density, and layer thicknesses as humans.[5] Vincelette *et al.* performed a study of 1070-nm continuous-wave laser MVL thresholds across exposure durations from 0.01 to 10 s and beam diameters of 0.6–9.5 cm.[6] DeLisi *et al.* extended this work by investigating exposures with 0.01, 0.1, and 10 s total laser on times (TOT), but broken up into multiple-pulse trains with various total numbers of pulses and duty cycles.[7] The given TOT is thus the sum of all the pulse durations within the exposure. This study also investigated single-pulse exposures of 0.01, 0.1, and 10 s on both shaved and waxed skin, demonstrating the mediating effect of highly absorbing hair follicles in lowering the damage threshold by almost a factor of 2 for the 0.01 s exposure duration cases, while showing no significant difference in the 10 s cases.[7] In one of the few recent examinations of submillisecond pulses, we found a threshold value of 0.74 J/cm$^2$ for a 10 ns pulse at a diameter of 0.8 cm for 1064 nm radiation in shaved porcine skin.[8]

Computational models are useful to examine the expected thermal response of biological tissue to laser irradiation,[9–11] along with the possibility and degree of induced damage by using the Arrhenius integral.[12–15] A typical laser tissue thermal response model must account for optical energy deposition, heat transfer, and damage assessment. These methods have been successful in the past, often in concert with *in vivo* threshold experiments for validation purposes. Oliver *et al.*,[16,17] Cain *et al.*,[18] and Zohner *et al.*[19] compare temperature response predictions from a computational model with experimental thermographic data collected during threshold studies at wavelengths of 1300–2000 nm, demonstrating good agreement. Chen *et al.* present a comprehensive thermal model of 2000 nm laser exposure to skin, employ it to simulate transient surface temperatures and thermal damage accumulation with the Arrhenius integral, and validate the results with experimental data.[9,20] These two studies also quantified thermal damage accumulation at the radial edges of laser skin lesions, similar to the approach of Denton *et al.* in measuring spatially correlated cell death boundaries *in vitro* for 514 nm (Ref. 21) and 532 nm (Ref. 22) laser exposures.

However, there are few reported efforts to model NIR laser skin interaction near the 1000 nm region, where water absorption is lower and scattering tends to be higher than at 1300–2000 nm. Initial attempts to replicate experimentally measured thermal profiles measured at the center of 1070-nm laser exposures to skin from DeLisi *et al.*[7] were unsuccessful. These efforts employed the BTEC software,[10] optical properties from Salomatina *et al.*,[23] and thermal and physical properties used by Oliver *et al.*,[16] to model 1319 nm exposures. A typical result can be seen in Fig. 1. As is evident, the modeled temperature change features significantly different characteristics, during both laser exposure and postexposure cooling.

We believe that the poor match between modeled and experimental temperature profiles in Fig. 1 is due to inaccuracies in values for tissue optical properties at this wavelength. Salomatina *et al.* report the optical absorption of the epidermis and dermis at 1070 nm to be 0.17 and 0.46 cm$^{-1}$, respectively.[23] However, these values are problematic, as the epidermis contains significant quantities of melanin, which is highly absorbing at 1070 nm compared to other chromophores, and should intuitively feature a higher absorption coefficient than the dermis. A recent study by Mignon *et al.*[24] confirms this, as the authors review a variety of reported theoretical and experimental skin optical properties, and determine that the Salomatina data does not align with known chromophore distributions. The resulting modeled temperature distribution seen in Fig. 1 can be explained by the minimal deposition of optical energy at the surface of the skin and the diffusion of heat upward from the highly absorbing dermis after the laser beam has been turned off.

Unfortunately, there are few other sources of epidermis optical properties in the literature outside of Salomatina *et al.* that include measurements taken in the NIR region. This could possibly be due to the difficulty in isolating the thin epidermis alone for measurement. The skin optical properties review article by Bashkatov *et al.*[25] references a few studies that measured human epidermis optical properties, but they were restricted to the visible light range.

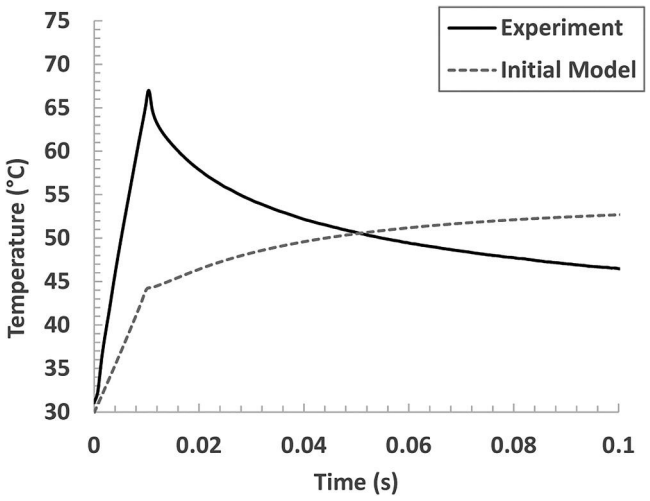


**FIG. 1.** Initial attempt to model 1070-nm laser exposure in porcine skin for a duration of 0.01 s, with a Gaussian beam diameter of 1 cm ($1/e^2$) and a laser power of 2780 W. This modeling effort employed optical properties from Salomatina *et al.* (Ref. 23).

Several widely cited skin optical properties studies that do include the NIR region, specifically 1070 nm, and utilize bulk skin tissue consisting of both the epidermis and dermis.[26,27] These values are not as useful for modeling scenarios with specific skin layer thicknesses.

Furthermore, most of these optical properties studies are for human skin, while most experiments employ porcine skin. Du *et al.* provide optical absorption and scattering coefficients between 900 and 1500 nm for the dermis of white domestic pigs, but they do not include epidermis measurements.[28] Cain *et al.* report optical absorption and scattering values between 1000 and 1600 nm for both the epidermis and dermis, but the data were collected from a single Yucatan mini-pig subject following laser exposures, after which the skin may have been irreversibly damaged.[29] Zamora-Rojas *et al.* also includes epidermis and dermis measurements, but in the range of 1150–2250 nm.[30]

Our aim is to present a model for NIR laser tissue exposure that accurately simulates the experimentally measured tissue thermal response, for both continuous-wave and multiple-pulse exposures, where the incorporation of thermal diffusion and relaxation between pulses is highly relevant. The model is comprised of three fundamental components: light propagation using Monte Carlo techniques, heat transfer through a solution to the Pennes bioheat equation, and damage quantification using the Arrhenius integral. Given the challenge in obtaining experimentally determined optical properties for porcine skin epidermis, we outline a method to derive a value for porcine epidermis absorption that meets the criteria for feasibility described by Mignon *et al.*[24] Furthermore, we present a set of Arrhenius rate process coefficients for quantification of skin damage to 1070-nm laser radiation, derived from experimental data using an original technique. These capabilities and innovations are leveraged to generate temperature histories and predict skin damage thresholds, which we then compare to experimental values from DeLisi *et al.*[7] The model does not incorporate hair follicle presence. Therefore, given the findings of DeLisi *et al.*,[7] we hypothesize that modeled thresholds will compare less favorably to shaved skin $ED_{50}$ data for the shorter, millisecond-scale exposure duration cases and more favorably for exposure durations on the scale of seconds or more. Similarly, we predict that comparisons to waxed skin $ED_{50}$ data will provide the most accurate validation.

## II. METHODS

The SCALABLE EFFECTS SIMULATION ENVIRONMENT (SESE) software program version 2.5.1a developed by Nanohmics (Austin, TX) implements the three necessary components of light propagation, heat transfer, and damage calculation. Details on the implementation and application of this software are expounded upon in a publically available technical report,[31] though we will briefly review the capabilities in Secs. II A–II C.

### A. Light propagation

The Monte Carlo method for radiative energy transport determines the spatial distribution of applied radiation in the object space. Radiation consists of a collection of rays, with an energy weight and directional vector, which emit in a Gaussian distribution. As a ray encounters a voxel in the object, it has a statistical chance to change direction (through scattering, reflection, or refraction), deposit energy (through absorption), or transmit to the next voxel along its vector. The optical properties of the material dictate these probabilistic interactions. SESE employs an implementation of the Monte Carlo radiative transport method that Prahl describes in detail.[32]

### B. Heat transfer

SESE models heat transfer in biological tissues using Pennes' bioheat equation, an expansion of the Fourier law of heat conduction,

$$\rho c \frac{\partial T}{\partial t} = \nabla(\kappa \nabla T) + q_s + q_b + q_m, \tag{1}$$

where $T$ is the temperature (°K), $t$ is the time (s), $\rho$ is the density (kg/m$^3$), $c$ is the specific heat (J/kg K), and $\kappa$ is the thermal conductivity (W/m K). The additional terms $q_s$, $q_b$, and $q_m$ represent heat loss or gains (W/m$^3$) due to a source (laser light, in this case), blood perfusion, and metabolic activity, respectively. The blood perfusion term expands as follows:

$$q_b = \omega \rho_b c_b (T_b - T). \tag{2}$$

$T_b$, $\rho_b$, and $c_b$ are the temperature, density, and specific heat of the perfused blood, respectively, while $\omega$ is the blood perfusion rate coefficient (s$^{-1}$).

Radiative, convective, and evaporative thermal flux boundary conditions are imposed at the object surface,

$$q_{rad} = \sigma \varepsilon (T^4 - T_\infty^4), \tag{3}$$

$$q_{conv} = h_{conv}(T - T_\infty), \tag{4}$$

$$q_{evap} = h_{evap}(p_{sat}(T) - RH \cdot p_{sat}(T_\infty)), \tag{5}$$

where $\sigma$ is the Stefan–Boltzmann constant (W/m$^2$ K$^4$), $\varepsilon$ is the surface emissivity (unitless), $h_{conv}$ is the convective heat transfer coefficient (W/m$^2$ K), $h_{evap}$ is the evaporative heat transfer coefficient (W/m$^2$ Pa), $T_\infty$ is the air temperature surrounding the object, and $RH$ is the relative humidity of the air (unitless). The function $p_{sat}(T)$ is the temperature-dependent saturation pressure of water vapor (Pa).

SESE solves the heat equation in a three-dimensional domain with a finite-volume voxel discretization by employing a Gauss–Seidel red-black successive over-relaxation method.[33]

### C. Damage rate

The Arrhenius rate equation describes temperature-dependent reaction rates, such as damage in tissue exposed to laser radiation. Give a temperature history at a given voxel location, and point in time $t$ during the history, the accumulated damage, $\Omega(t)$, is

expressed as

$$\Omega(t) = A \int_0^t \exp\left(-\frac{E_a}{RT(t')}\right) dt'. \quad (6)$$

$R$ is the gas constant of 8.314 J/K mol, $E_a$ is the denaturation activation energy (J/mol), and $A$ is the molecular collision frequency factor ($s^{-1}$), or the Arrhenius prefactor. Henriques and Moritz[12,15] assigned a value of $\Omega = 1$ to the threshold for epidermal necrosis, which corresponds to ~63% of the material experiencing the temperature history being damaged. Historically, investigators in laser bioeffects have associated a value of $\Omega = 1$ with the MVL threshold.[9,16–18]

$E_a$ and $A$ vary widely for different materials, although several studies have produced values for skin. Oliver *et al.*[17] favored the classic rate process coefficients by Henriques,[12] while Chen *et al.*[20] explored a variety of coefficients including those from Wu,[34] which are essentially an update to the Henriques values at temperatures greater than 53 °C. Note that the Wu[34] coefficients are unpublished but are referenced and explained by Palla[35] and further referenced in the widely cited compilation of thermal damage and rate process parameters by Thomson and Pearce.[36] These rate process coefficients come from studies that defined threshold damage as complete trans-epidermis necrosis. This is not the same as the less severe MVL metric, which typically manifests as barely visible erythema on the epidermis surface. Furthermore, the studies by Chen *et al.* note that their most accurate simulated damage thresholds correspond to calculating the Arrhenius integral at varying depths within tissue, depending on laser parameters such as exposure time and beam diameter.[9,20]

Our initial attempts to employ published rate process coefficients to simulate and predict MVL $ED_{50}$ thresholds using the temperature on the skin surface had mixed results, with the percent difference with the experimental thresholds varying nonmonotonically with laser exposure parameters. With the goal of maximizing the accuracy of modeled threshold predictions, where the MVL $ED_{50}$ is the gold standard, we derived a new set of rate process coefficients, $E_a$ and $A$, using $ED_{50}$ values and accompanying skin surface thermographic recordings from our previous study of 1070-nm laser damage thresholds in porcine skin.[7] The technique for generating these custom rate process coefficients is unique. We have described them in detail with appropriate context in the Appendix of this paper, with the computer code available for public use at https://github.com/CD3/libArrhenius.

This process required skin surface temperature profiles at known exposure thresholds as inputs. We used three exposures from waxed subjects at 0.01, 0.1, and 10 s continuous-wave exposure times that were near to their respective $ED_{50}$ value. We selected these temperature profiles such that their peak temperature change with respect to laser irradiance, or thermal slope, was in agreement with the linear fit to all of the collected data at the given exposure duration. The method for determining these thermal slopes is more thoroughly explained by DeLisi *et al.*[7] The temperature profiles were then scaled to the peak temperature at the $ED_{50}$ irradiance predicted by the linear fit, holding their starting temperatures constant. We considered this scaled profile to be an appropriate representation of the average temperature response at the $ED_{50}$ for the data set. Figure 2 shows the peak temperature change data for 0.1 s waxed exposures, along with the linear fit to the data, the expected peak temperature change at the $ED_{50}$, and the data point selected for thermal profile scaling. The resulting values for $E_a$ and $A$ using our technique, along with those from Henriques and Wu, are listed in Table I.

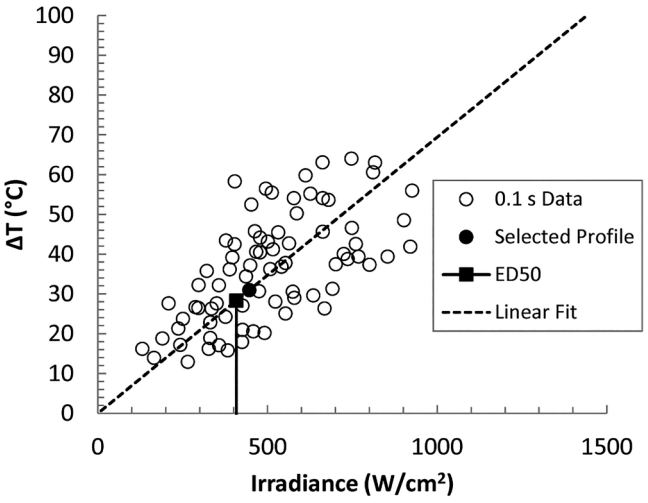


**FIG. 2.** Example of peak temperature change data from 0.1 s single-pulse exposures. The linear fit defines the thermal slope for the given parameter set. The selected temperature profile along this line was scaled down to the $ED_{50}$ level and then used as an input for the calculation of Arrhenius rate process coefficients.

## D. Simulation configuration

Tables II and III provide the specific tissue and environmental parameters used to model 1070-nm laser skin thermal response. The values in these tables are assumed to be the static values at 20 °C, with temperature-dependent dynamic formulations for the layer thermal properties implemented within the model. This section expands upon the rationale for each value chosen.

**TABLE I.** Rate process coefficients used to quantify damage accumulation with the Arrhenius integral.

| Source | Temperature range (°C) | $A$ (s−1) | $E_a$ (J/mol) |
|---|---|---|---|
| Henriques (Ref. 12) | All $T$ | $3.1 \times 10^{98}$ | $6.27 \times 10^5$ |
| Wu (Ref. 34) | $T \leq 53$ | $3.1 \times 10^{98}$ | $6.27 \times 10^5$ |
| | $T > 53$ | $3.1 \times 10^{98}$ | $[6.27–0.0051 \times (T - 53)] \times 10^5$ |
| This work | All $T$ | $2.74 \times 10^{94}$ | $5.90 \times 10^5$ |

**TABLE II.** Summary of layer-specific physical properties used in the model. The values for density, specific heat, and thermal conductivity are for 20 °C.

| Property | Units | Layer | Value | Reference |
|---|---|---|---|---|
| Thickness | mm | Epidermis | 0.082 | 37 |
| | | Dermis | 2.7 | 37 |
| | | Fat | 15 | — |
| Optical absorption coefficient, $\mu_a$ | $cm^{-1}$ | Epidermis | 0.35 | — |
| | | Dermis | 0.17 | 28 |
| | | Fat | 1.03 | 26 |
| Reduced scattering coefficient, $\mu_s'$ | $cm^{-1}$ | Epidermis | 17.4 | 38 |
| | | Dermis | 15.4 | 28 |
| | | Fat | 8.94 | 26 |
| Water fraction, $w$ | — | Epidermis | 0.3 | 9 and 17 |
| | | Dermis | 0.8 | 9 and 17 |
| | | Fat | 0.2 | 39 |
| Density, $\rho$ | $kg/m^3$ | Epidermis | 1210 | 17 and 40 |
| | | Dermis | 1060 | 17 and 40 |
| | | Fat | 850 | 41 |
| Specific heat, $c$ | J/kg K | Epidermis | 2244 | 17 and 40 |
| | | Dermis | 3663 | 17 and 40 |
| | | Fat | 2070 | 42 |
| Thermal conductivity, $\kappa$ | W/m K | Epidermis | 0.20 | 17 and 40 |
| | | Dermis | 0.49 | 17 and 40 |
| | | Fat | 0.16 | 42 |
| Blood perfusion rate, $\omega$ | $s^{-1}$ | Epidermis | 0 | — |
| | | Dermis | $1.25 \times 10^{-3}$ | 43 |
| | | Fat | $1.25 \times 10^{-3}$ | 43 |

The skin model consisted of a three-dimensional cubic structure, composed of a thin surface epidermis layer, a middle dermis layer, and a base of subcutaneous fat. The spatial domain of the model covered a quarter of the exposed area, with the origin at the center of the beam and two symmetry planes in order to reduce simulation time. The thicknesses of the epidermis and dermis were set to average values for female Yucatan miniature pigs between the ages of 4 and 5.4 months,[37] while the fat layer thickness was specified to a value large enough to provide a thermal sink.

**TABLE III.** Boundary condition parameters, damage rate coefficients, and nonlayer specific properties used in the model.

| Property | Units | Value | Reference |
|---|---|---|---|
| Room temperature, $T_\infty$ | K | 20 | — |
| Relative humidity, $RH$ | — | 0.5 | — |
| Emissivity, $\varepsilon$ | — | 0.98 | 44 |
| Convective heat transfer coefficient, $h_{conv}$ | $W/m^2$ K | 10 | 9 and 45 |
| Evaporative heat transfer coefficient, $h_{evap}$ (32 °C) | $W/m^2$ Pa | 0.0974 | 9 |
| Blood density, $\rho_b$ | $kg/m^3$ | 1060 | 46 |
| Blood specific heat, $c_b$ | J/kg K | 3770 | 46 |
| Metabolic heat, $q_m$ | $W/m^3$ | 368.1 | 46 |

The epidermis layer was subject to radiative, convective, and evaporative boundary conditions. The radiative condition is subject to the emissivity of the skin, which is 0.98.[44] The convective coefficient was set to 10 $W/m^2$ K, which agrees with typical values for free convection in air.[45] We employed the framework outlined by Chen *et al.*[9] for determination of the evaporative coefficient, which is dependent on the static convective coefficient, the temperature-dependent density and specific heat of air, and the difference between the mass density of saturated water vapor at the tissue surface and the air. This resulted in an evaporative coefficient value of 0.0974 $W/m^2$ Pa at an approximate resting skin surface temperature of 32 °C, rising to 0.1125 $W/m^2$ Pa at 45 °C, and falling to 0.0504 $W/m^2$ Pa at 99 °C.

In order to derive a value for the optical absorption coefficient of porcine epidermis based on chromophore distribution as suggested by Mignon *et al.*,[24] we employ the framework suggested by Jacques.[47] This approach breaks down the optical absorption of the tissue as a sum of the absorption of its primary chromophores, scaled by their fractional contribution to the tissue volume. For epidermis in the visible and near-infrared range, we isolate the components to melanin and a remainder baseline value. In a review of the optical properties of biological tissues, Jacques provides several wavelength-dependent functions to calculate melanosome optical absorption based on power function fits to data from various studies.[48] Given that our past experiments utilized Yucatan miniature pig subjects,[7] we rely on the data from Sherwood *et al.*, which provide values for the optical absorption coefficient of melanosomes in miniature pigs for several wavelengths between 504 and 750 nm.[49] The ensuing power function fit is

$$\mu_{a,mel} = (4.9 \times 10^{15})(\lambda^{-4.806}), \tag{7}$$

where $\mu_{a,mel}$ is the optical absorption coefficient of melanosomes in $cm^{-1}$ and $\lambda$ is the wavelength of the laser in nm. For 1070 nm, this results in an optical absorption coefficient of 13.5 $cm^{-1}$. Vincelette *et al.* determined that the epidermis in Yucatan miniature pigs contains 0.81% melanin by volume.[50] When combined with the proportionate remainder baseline melanin-less epidermis tissue from Jacques,[47] the resulting optical absorption coefficient of the miniature pig epidermis is 0.35 1/cm.

The reduced scattering coefficient of the epidermis was derived from wavelength-dependent equations presented by Altshuler *et al.*,[38] a study that Mignon *et al.*[24] conclude aligns with expected chromophore distributions. Optical properties of the dermis were taken from Du *et al.*, which is one of the only studies that specifically measured absorption and scattering of porcine dermis in the near-infrared range.[28] Bashkatov *et al.* provided values for the optical absorption and reduced scattering of subcutaneous fat tissue.[26]

We utilize the same thermal properties for epidermis and dermis as our past efforts[17] that are derived from equations from Takata *et al.*[40] These equations rely on an understanding of the water content of the tissues, which we assume to be 80% in the dermis and 30% in the epidermis, as do Oliver *et al.*[17] and Chen *et al.*[9] Thermal properties and water content of the subcutaneous fat tissue are taken from a variety of sources.[39–42]

The aforementioned tissue physical properties are valid for the static case, typically measured from excised tissue at or around room temperature of 20 °C. However, tissue physical properties are dynamic by nature, featuring transient changes with respect to environmental variables such as temperature and pressure. Furthermore, tissue properties may change after experiencing permanent damage, such as protein denaturation due to elevated temperature that will persist even after the temperature returns to its starting point. SESE is capable of implemented both temperature- and damage-dependent physical properties. Unfortunately, there are very few studies of biological tissue properties that track their values over temperature or degrees of accumulated damage through the Arrhenius integral.

In an effort to capture some degree of the dynamics of thermal properties, we consider each tissue type to be a mixture of water and nonwater components,

$$x_T = (w)(x_{w,T}) + (1 - w)(x_0), \tag{8}$$

where $x_T$ is the thermal property (density, specific heat, or thermal conductivity) of the tissue at temperature $T$, $w$ is the water fraction of the tissue, $x_{w,T}$ is the thermal property of water at temperature $T$, and $x_0$ is the net baseline thermal property of the nonwater, or "dry," components of the tissue that does not change with temperature. To calculate the value of $x_0$ for each tissue type, we substitute the static thermal property value obtained from the literature for $x_T$ at $T = 20$ °C, as we assume that most measurements of these properties are taken at room temperature. We have cited sources for the water fractions of each tissue, and the temperature-dependent thermal properties of water are very well documented.[51,52] With $x_0$ determined using the static tissue thermal property value at $T = 20$ °C, we can subsequently employ the water tables to calculate the dynamic tissue thermal property $x_T$ at any temperature. Note that the temperature-dependent properties of water are also pressure-dependent, so we assume standard atmospheric pressure of 0.1 MPa for all values.

We did not implement temperature- or damage-dependent optical properties of tissues, as these trends are currently understudied. Roggan *et al.* did investigate the differences in the near-infrared absorption and scattering coefficients of various internal organs in the native and "coagulated" states, with this damaged end point defined as immersion in a 75 °C water bath for an unspecified amount of time.[53] They found that the optical absorption changes are relatively minor, while the scattering coefficient increases in the damaged state. Zhou *et al.* implemented these damage-dependent optical properties as well as temperature-dependent thermal properties in the simulation of laser-induced thermotherapy of liver tumors.[54] They found that when compared to the static material property case, the implementation of temperature-dependent thermal properties had a greater effect on tissue temperature rise than incorporation of damage-dependent optical properties.

## III. RESULTS

### A. Thermal response

Figure 3 is an example of a three-dimensional temperature distribution output of the model, taken after 0.01 s of laser exposure at 2780 W with a Gaussian beam diameter of 1 cm ($1/e^2$). The highest temperature region was at the surface epidermis layer, due to the presence of melanin, which absorbs more at this wavelength than other chromophores. The dermis featured low absorption and high scattering, resulting in significant light energy penetrating through to the fat tissue. This allowed the highly absorbing fat to experience a greater temperature increase than the dermis.

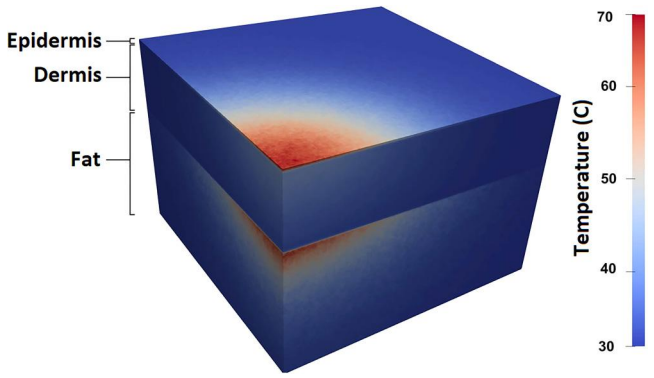


**FIG. 3.** Model output after 0.01 s laser exposure at 2780 W and 1 cm beam diameter ($1/e^2$). The displayed three-dimensional domain is a cube with side length of 0.7 cm and represents a quadrant of the beam.

We compared the results of the computational model at a given set of laser parameters with thermal imagery extractions from the experimental data. The temperature histories for both the recorded and modeled thermal response are from the center of the beam. Figures 4 and 5 show comparisons of experimentally measured and modeled temperatures during and after laser exposure, using data from DeLisi *et al.*[7] for 0.01 and 10 s TOTs. The experimental data shown in these figures were all from the same subject, minimizing possible biological differences in tissue optical properties from pigment or skin layer thicknesses. The single-pulse, continuous-wave exposures were from a waxed area of the subject, where the entire hair follicle was removed, while the multiple-pulse exposures were from regions where the hair was simply shaved.

Figure 4 demonstrates good agreement of the models with the experimental data for continuous-wave, single-pulse exposures. The model of the 0.01-s exposure in Fig. 4(a) slightly underestimated the peak temperature and slightly overestimated the postexposure temperature, while the model of the 10 s exposure in Fig. 4(b) followed the experimental thermal profile well over the laser on time and the cooling period.

Figure 5 shows that the model also performed well for multiple-pulse exposure scenarios where accounting for the thermal relaxation between pulses is a key concern. The modeled 0.01-s TOT multiple-pulse exposure in Fig. 5(a) featured a slightly higher peak temperature at the end of the pulse train than the experimental thermal extraction, but was otherwise accurate in terms of temperature growth and decay rates. The discrepancy in peak temperature was not surprising, due to the possible presence of local highly absorbing hair follicles that can influence transient

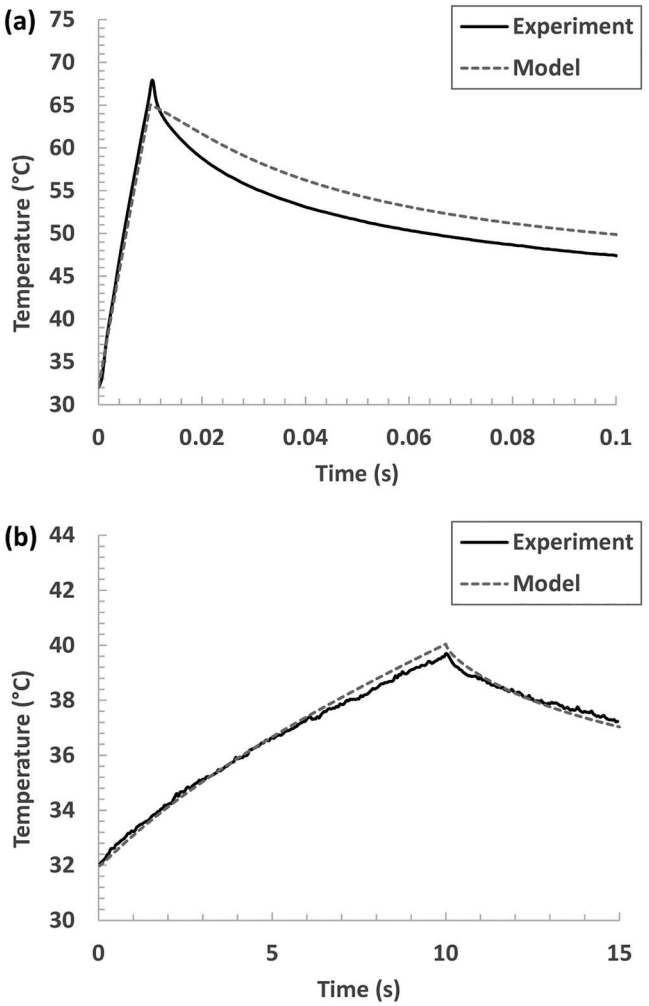


**FIG. 4.** Modeled and experimental thermal data at the center of a beam for (a) a 0.01-s single-pulse exposure at 2780 W with a 1.04 cm beam diameter ($1/e^2$) and (b) a 10-s single-pulse exposure at 3.11 W with a 0.973 cm beam diameter ($1/e^2$). The experimental data are from DeLisi *et al.* (Ref. 7).

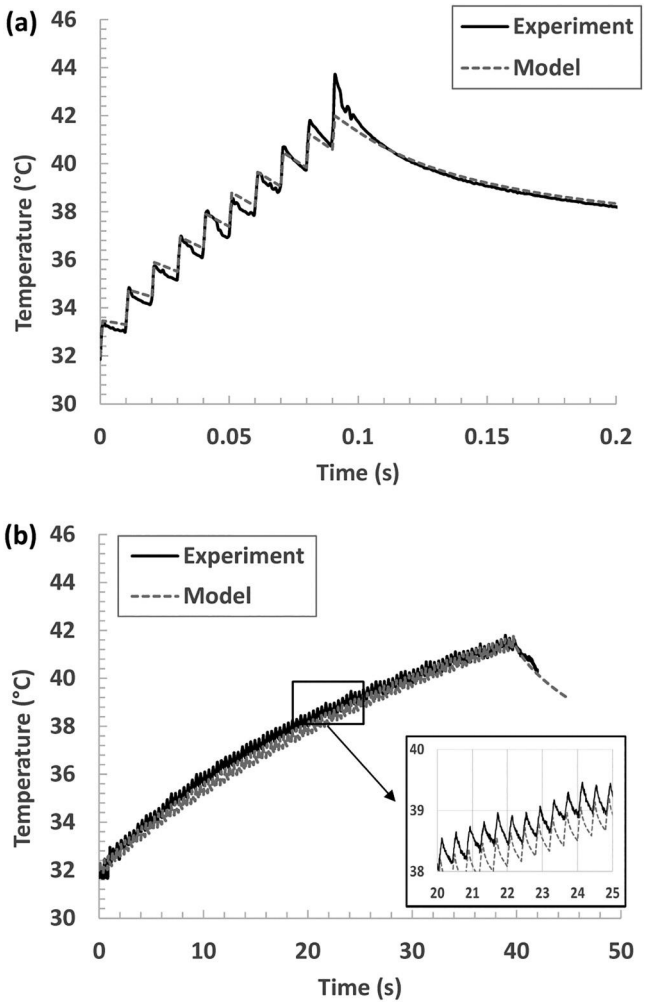


**FIG. 5.** Modeled and experimental thermal data at the center of the beam for (a) a 10-pulse, 10% duty cycle exposure at 2780 W with 0.01 s TOT and a 1.04 cm beam diameter ($1/e^2$) and (b) a 100-pulse, 25% duty cycle exposure at 6.29 W with 10 s TOT and a 0.973 cm beam diameter ($1/e^2$). The experimental data are from DeLisi *et al.* (Ref. 7).

temperatures. The 10-s TOT multiple-pulse exposure shown in Fig. 5(b) also shows good agreement between the model and the experimental data, with minor differentiation in the middle of the exposure. The agreement of modeled and experimental temperature profiles implies that our employed values for skin epidermis and dermis optical properties were more realistic than those presented by Salomatina *et al.*[23] This was specifically due to a more realistic representation of the absorption difference between the melanin-rich epidermis and dermis.

### B. Damage threshold prediction

Model-generated tissue thermal response to laser exposure allows for prediction of damage thresholds for given laser parameter sets. Specifically, the modeled threshold is the laser radiant exposure necessary to produce a temperature history in the center of the beam that results in $\Omega = 1 \pm 0.2$ from Eq. (6). We computed the Arrhenius integral over the modeled temperature profile from the onset of the laser exposure until after the exposure when the temperature has fallen to the 37% ($1/e$ level) of the peak value. This allowed for incorporation of some of the cooling time in the Arrhenius calculation. The error condition of ±0.2 permitted earlier convergence of the threshold search, as repetitive simulations could become computationally expensive, particularly for the longer duration exposures with multiple pulses. We provided three thresholds for each parameter set, using rate process coefficients from Henriques[12] and Wu,[34] along with those from this work that

**TABLE IV.** Model results compared to 24-h MVL radiant exposure $ED_{50}$ values due to a single 1070-nm laser pulse, for shaved and waxed skin, from DeLisi *et al.* (Ref. 7).

| Waxed or shaved? | Beam diameter ($1/e^2$) (cm) | Pulse duration (s) | Radiant exposure $ED_{50}$ ($J/cm^2$) | Modeled threshold ($J/cm^2$) | | | Percent difference (%) | | |
|---|---|---|---|---|---|---|---|---|---|
| | | | | This work | Henriques (Ref. 12) | Wu (Ref. 34) | This work | Henriques (Ref. 12) | Wu (Ref. 34) |
| Shaved | 1.04 | 0.01 | 17.8 | 28.3 | 35.5 | 32.6 | 45.5 | 66.5 | 58.8 |
| Shaved | 1.04 | 0.1 | 33.2 | 35.8 | 48.0 | 40.9 | 7.5 | 36.5 | 20.8 |
| Shaved | 0.973 | 10 | 83.7 | 94.5 | 126.1 | 120.1 | 12.2 | 40.4 | 35.8 |
| Waxed | 1.04 | 0.01 | 27.2 | 28.3 | 35.5 | 32.6 | 3.9 | 26.6 | 18.2 |
| Waxed | 1.04 | 0.1 | 40.8 | 35.8 | 48.0 | 40.9 | 13.1 | 16.2 | 0.3 |
| Waxed | 0.973 | 10 | 85.9 | 94.5 | 126.1 | 120.1 | 9.6 | 37.9 | 33.2 |
| Average | | | | | | | 15.3 | 37.3 | 27.9 |

we custom generated as outlined in Sec. II C. As a validation check for our model, we referenced 24-h MVL damage thresholds from 1070-nm laser exposure from DeLisi *et al.*[7] and calculated the percent difference between the $ED_{50}$ and the model result using the given rate process coefficient.

Table IV contains continuous-wave, or single-pulse, MVL data from DeLisi *et al.*[7] for waxed and shaved porcine skin, along with the modeled results for the given exposure times. Multiple-pulse exposures were grouped according to their laser total on times of 0.01, 0.1, and 10 s in Tables V–VII, respectively. The number of pulses, pulse duration, and duty cycle defines the parameters for each pulse train. The total sequence duration is the time from the onset of the first pulse and the falling edge of the last pulse. All multiple-pulse $ED_{50}$ thresholds provided by DeLisi *et al.* were for shaved porcine skin, where the hair was trimmed from the surface but the base of the follicle was still present.[7]

The hair follicles in shaved exposures served as local, intense heat sources at the skin surface since they are highly absorbing at 1070 nm. DeLisi *et al.*[7] observed them to skew the MVL thresholds downward such that less laser energy is required to observe a visible change. Figure 6 shows the comparisons between the shaved, waxed, and modeled thresholds. The model aligned very well with the waxed $ED_{50}$ data for all three exposure duration time points on a logarithmic scale, while diverged from the shaved data significantly at 0.01 s. This behavior confirmed our hypothesis that the model demonstrates higher accuracy when compared to the waxed case, given that it did not incorporate highly absorbing hair follicles in its skin object structure.

## IV. DISCUSSION

### A. Retrospective modeling

Figures 4 and 5 exhibit seemingly accurate temperature profile matches between experimentally collected thermography on the skin surface and extractions from the top layer of the model. We present these images to demonstrate the robustness of the model performance across short (0.01 s) and long (10 s) laser on times, for the continuous-wave case and the multiple-pulse case, respectively. The experimental profiles are good approximations of the typical temperature response seen in experiments for their given parameter sets, although there is disparity from exposure to exposure. Biological variation is a key contributor to these disparities, such as changes in melanin density distribution, skin layer thickness, and degrees of stratum corneum exfoliation. These factors

**TABLE V.** Model results compared to 24-h MVL total radiant exposure $ED_{50}$ values due to 1070-nm laser pulses with a beam diameter of 1.04 cm, for shaved skin. The laser total on time for each set of parameters is 0.01 s.

| Number of pulses | Pulse duration (ms) | Duty cycle (%) | Total sequence duration (s) | Radiant exposure $ED_{50}$ ($J/cm^2$) | Modeled threshold ($J/cm^2$) | | | Percent difference (%) | | |
|---|---|---|---|---|---|---|---|---|---|---|
| | | | | | This work | Henriques (Ref. 12) | Wu (Ref. 34) | This work | Henriques (Ref. 12) | Wu (Ref. 34) |
| 10 | 1 | 50 | 0.019 | 17.6 | 29.4 | 37.4 | 34.1 | 50.3 | 72.0 | 63.8 |
| 10 | 1 | 25 | 0.037 | 18.6 | 31.3 | 40.1 | 36.4 | 50.9 | 73.3 | 64.7 |
| 10 | 1 | 10 | 0.091 | 20.0 | 38.8 | 48.1 | 42.9 | 63.8 | 82.4 | 72.8 |
| 30 | 0.333 | 50 | 0.0197 | 17.2 | 29.2 | 36.5 | 33.0 | 51.7 | 71.9 | 62.8 |
| 30 | 0.333 | 25 | 0.039 | 17.3 | 30.7 | 38.5 | 35.3 | 55.9 | 75.9 | 68.5 |
| 30 | 0.333 | 10 | 0.097 | 19.7 | 36.6 | 44.7 | 39.3 | 59.9 | 77.6 | 66.3 |
| 100 | 0.1 | 50 | 0.0199 | 15.6 | 29.4 | 36.5 | 33.9 | 61.3 | 80.2 | 73.9 |
| 100 | 0.1 | 25 | 0.0397 | 16.9 | 30.7 | 38.9 | 36.0 | 58.1 | 78.7 | 72.1 |
| 100 | 0.1 | 10 | 0.0991 | 18.0 | 36.1 | 44.6 | 41.2 | 66.9 | 85.0 | 78.4 |
| Average | | | | | | | | 57.6 | 77.4 | 69.3 |

**TABLE VI.** Model results compared to 24-h MVL total radiant exposure $ED_{50}$ values due to 1070-nm laser pulses with a beam diameter of 1.04 cm, for shaved skin. The laser total on time for each set of parameters is 0.1 s.

| Number of pulses | Pulse duration (ms) | Duty cycle (%) | Total sequence duration (s) | Radiant exposure $ED_{50}$ ($J/cm^2$) | Modeled threshold ($J/cm^2$) | | | Percent difference (%) | | |
|---|---|---|---|---|---|---|---|---|---|---|
| | | | | | This work | Henriques (Ref. 12) | Wu (Ref. 34) | This work | Henriques (Ref. 12) | Wu (Ref. 34) |
| 10 | 10 | 50 | 0.19 | 38.2 | 40.8 | 51.7 | 47.4 | 6.6 | 30.1 | 21.4 |
| 10 | 10 | 25 | 0.37 | 41.6 | 46.8 | 58.4 | 54.7 | 11.8 | 33.5 | 27.1 |
| 10 | 10 | 10 | 0.91 | 52.6 | 55.0 | 69.0 | 64.1 | 4.4 | 27.0 | 19.7 |
| 30 | 3.33 | 50 | 0.197 | 37.4 | 39.7 | 51.3 | 47.1 | 6.0 | 31.4 | 22.9 |
| 30 | 3.33 | 25 | 0.39 | 38.2 | 46.7 | 58.9 | 54.5 | 20.0 | 42.6 | 35.2 |
| 30 | 3.33 | 10 | 0.97 | 49.5 | 55.6 | 70.8 | 66.7 | 11.6 | 35.4 | 29.6 |
| 100 | 1 | 50 | 0.199 | 38.0 | 41.2 | 51.5 | 47.7 | 8.1 | 30.2 | 22.6 |
| 100 | 1 | 25 | 0.397 | 43.7 | 47.7 | 59.5 | 54.5 | 8.7 | 30.6 | 22.0 |
| 100 | 1 | 10 | 0.991 | 48.8 | 55.6 | 71.0 | 66.7 | 13.1 | 37.0 | 31.0 |
| Average | | | | | | | | 10.0 | 33.1 | 25.7 |

certainly change across different porcine subjects but also vary across the flank of one given subject. However, the static model parameters and their temperature-dependent formulations do not change from exposure to exposure.

In order to assess the model performance with respect to the whole data set, Fig. 7 plots the changes in peak temperature against laser irradiance for the continuous-wave waxed experimental data. We also provide the modeled change in temperature at three irradiance points at the low-, mid-, and high-end of the irradiances used in experiments. The linear fit to the data followed the process described by DeLisi *et al.*[7] to filter out the effects of extreme hot spots such as incineration events. The linear fit for the model was using the three aforementioned points, along with a forced y-intercept of zero to ensure that there was no expected temperature rise without an incident irradiance. The slopes of the linear fits for the experimental data and the model are in Table VIII.

As can be seen for each case in Fig. 7, the experimental distribution of temperature changes for a given exposure irradiance was quite broad. The linear fits to the experimental data serve as the best approximation of the representative temperature response to irradiance. However, the model returned a very consistent temperature response across the entire range of experimental irradiances. Visual inspection of each plot in Fig. 7 suggests that the modeled response was in good agreement with the linear fit of the experimental data, especially for the 0.1 and 10 s exposure time cases. The percent difference between the modeled and experimental data linear fits listed in Table VIII provides a metric for comparison. The small percent difference in the 0.1 s (4.8%) and 10 s (1.7%) cases confirmed the visual assessment provided by the figure. A percent difference in the slopes of 14% for the 0.01 s case is still

**TABLE VII.** Model results compared to 24-h MVL total radiant exposure $ED_{50}$ values due to 1070-nm laser pulses with a beam diameter of 0.973 cm, for shaved skin. The laser total on time for each set of parameters is 10 s.

| Number of pulses | Pulse duration (s) | Duty cycle (%) | Total sequence duration (s) | Radiant exposure $ED_{50}$ ($J/cm^2$) | Modeled threshold ($J/cm^2$) | | | Percent difference (%) | | |
|---|---|---|---|---|---|---|---|---|---|---|
| | | | | | This work | Henriques (Ref. 12) | Wu (Ref. 34) | This work | Henriques (Ref. 12) | Wu (Ref. 34) |
| 10 | 1 | 80 | 12.25 | 86.6 | 102.8 | 135.3 | 128.5 | 17.1 | 43.9 | 39.0 |
| 10 | 1 | 50 | 19 | 94.8 | 115.8 | 152.1 | 147.9 | 19.9 | 46.4 | 43.8 |
| 10 | 1 | 25 | 37 | 126 | 143.0 | 189.9 | 180.8 | 12.6 | 40.4 | 35.7 |
| 30 | 0.333 | 80 | 12.42 | 79.9 | 103.9 | 134.5 | 128.5 | 26.1 | 50.9 | 46.7 |
| 30 | 0.333 | 50 | 19.67 | 97.4 | 117.7 | 156.2 | 147.9 | 18.9 | 46.3 | 41.2 |
| 30 | 0.333 | 25 | 39 | 120 | 148.1 | 200.1 | 189.9 | 21.0 | 50.1 | 45.1 |
| 100 | 0.1 | 80 | 12.48 | 77.9 | 103.0 | 133.1 | 129.1 | 27.8 | 52.4 | 49.5 |
| 100 | 0.1 | 50 | 19.9 | 100 | 117.7 | 156.2 | 147.9 | 16.3 | 43.8 | 38.7 |
| 100 | 0.1 | 25 | 39.7 | 121 | 151.0 | 195.1 | 189.9 | 22.1 | 46.9 | 44.3 |
| Average | | | | | | | | 20.2 | 46.8 | 42.7 |

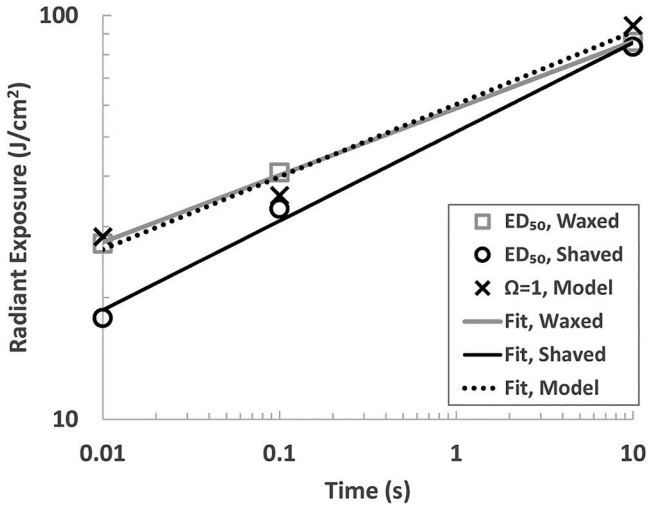


**FIG. 6.** Experimental MVL $ED_{50}$ values of waxed and shaved porcine skin from DeLisi *et al.* (Ref. 7) for a 1 cm beam diameter ($1/e^2$), and the thresholds determined by the model. The plotted data are available in Table IV.

low but highlights the increased noisiness of the temperature response data at lower time durations.

A closer inspection of Fig. 7(a) reveals that the modeled response underestimated the experimental data linear fit but seems to be in better agreement with the data points on the lower end of the irradiance range. This feature is in agreement with our hypothesis that some of the high temperature changes for the 0.01 s parameter set could be due to incidents of extreme local absorption, such as dense melanin patches, subsurface hair follicles, or small incineration events. While these local absorbers will also be present in the longer exposure cases, the higher irradiances featured in the 0.01 s cases result in heat accumulation within the local absorbers at a rate that is faster than their ability to diffuse it, resulting in the more drastic changes in peak temperature.

Note that the experimental temperature responses in Fig. 7 are from waxed exposures, which have presumably removed all of the highly absorbing hair follicles from the surface. Figure 7 and Table VIII demonstrated good agreement between the modeled and representative experimental temperature responses, as expected since the model did not include hair follicles. Figure 6 demonstrated that the modeled threshold values also aligned well with the waxed $ED_{50}$ values but diverged from the shaved $ED_{50}$ values as the exposure duration decreased. Given these relationships, we expect the multiple-pulse modeled threshold predictions to compare less favorably with the $ED_{50}$ thresholds at 0.01 s TOT, where the effects of hair follicles are most relevant.

We compared the modeled threshold predictions with the experimental 24-h $ED_{50}$s from DeLisi *et al.*[7] by plotting the percent difference between the two for each exposure parameter against the total sequence duration in Fig. 8. This plot displays the percent differences for each of the three rate process coefficients employed for threshold calculation. The figure contains the single- and multiple-

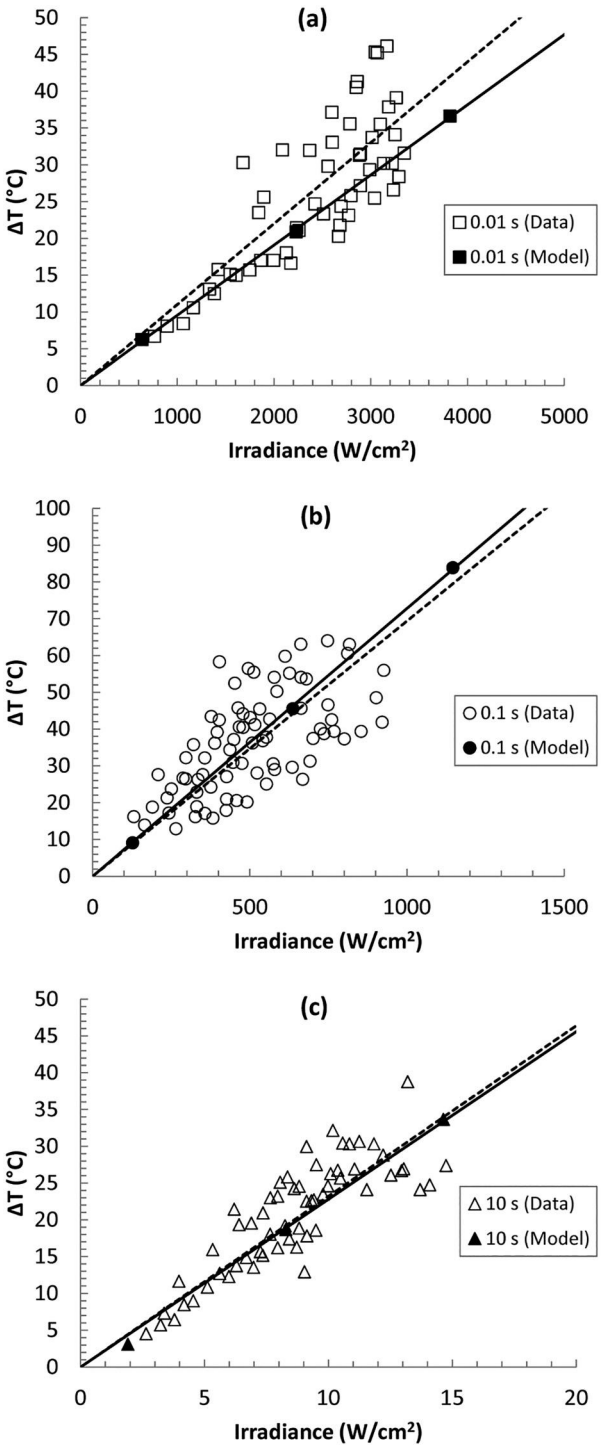


**FIG. 7.** Modeled and experimental change in peak temperatures after (a) 0.01, (b) 0.1, and (c) 10 s single-pulse laser exposure to waxed porcine skin. The dotted line is the linear fit to the experimental data, while the solid line is the linear fit to the model.

**TABLE VIII.** Slopes of the linear fits to temperature change vs laser irradiance plots, for experimental data and model.

| Exposure time (s) | Beam diameter ($1/e^2$) (cm) | $\Delta T$ slope, data (°C cm$^2$/W) | $\Delta T$ slope, model (°C cm$^2$/W) | Percent difference (%) |
|---|---|---|---|---|
| 0.01 | 1.04 | 0.0110 | 0.009 54 | 14 |
| 0.1 | 1.04 | 0.0694 | 0.0728 | 4.8 |
| 10 | 0.973 | 2.32 | 2.28 | 1.7 |

pulse data, with the 0.01 s TOT cases having total sequence durations between 0.01 and 0.1 s, the 0.1 s TOT cases having total sequence durations between 0.1 and 1 s, and the 10 s TOT cases having total sequence durations between 10 and 40 s. The percent differences for the waxed data for 0.01, 0.1, and 10 s are also included in this plot. The lines are a simple logarithmic function fit to the percent differences between the waxed data and the model of the form $y = a \ln x + b$, where $y$ is the percent difference (%) and $x$ is the total sequence duration (s). Since the temperature changes produced by the model matched fairly well with the representative temperature response of the waxed exposures, these lines are a good metric for gauging both the effect of hair follicles on the thresholds and the ability of the rate process coefficients to predict an accurate threshold.

Figure 8 shows relatively high percent difference between the shaved $ED_{50}$ and modeled thresholds for the 0.01 s TOT cases. The difference decreased substantially for the 0.1 s TOT cases and then slightly rose again for the 10 s TOT cases. We attribute this high percent difference at 0.01 s TOT to the presence of hair follicles. The waxed data at 0.01 s TOT featured significantly less percent difference than their shaved counterparts, for each rate process coefficient, given that the model did not account for highly absorbing hair follicles.

Note that the model results varied depending on the rate process coefficient used to calculate $\Omega = 1 \pm 0.2$. Upon inspection, Fig. 8 clearly demonstrates that the percent difference between the experimental and modeled thresholds is the lowest using the rate process coefficients from this work, followed by the Wu[34] coefficients and finally the Henriques[12] coefficients. This relationship was true across all total sequence durations and for each TOT grouping, as was confirmed by the average percent differences for each rate process coefficient in Tables IV–VII.

The logarithmic function fits to the percent difference between the waxed $ED_{50}$ and the modeled thresholds are a useful visual indicator and more genuine assessment of model performance, as they represent the most analogous comparison of data points. Their amplitude and distribution relative to each other is also an indicator of the appropriateness of the given rate process coefficients. The custom coefficients from this work was again confirmed to feature the lowest percent difference, followed by Wu and then Henriques, mirroring the trends from the shaved data distributions. The logarithmic fits using the Wu and Henriques values also featured a slight upward slope, with the highest percent difference being at 10 s. This is in contrast to the logarithmic fit to the waxed percent differences using the custom rate process coefficients from this work, which featured a relatively flat slope.

These behaviors indicate that the Wu and Henriques coefficients were not appropriate for the longer time duration exposures from DeLisi *et al.*[7] and demonstrated the need to generate custom rate process coefficients that hold across exposure duration. We expected lower percent differences and flatter logarithmic fit to the waxed data using the custom coefficients from this work, as they were generated using damage $ED_{50}$ thresholds and temperature

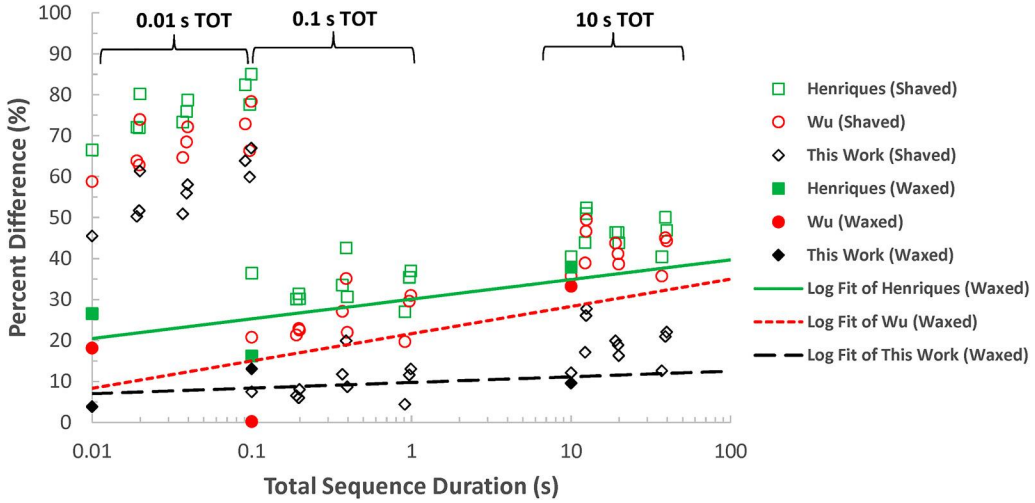


**FIG. 8.** Percent difference between the experimental $ED_{50}$ and modeled threshold over total sequence duration. The data groupings of 0.01, 0.1, and 10 s TOT are indicated by the top brackets. Model results are shown using rate process coefficients from Henriques (Ref. 12) and Wu (Ref. 34), along with the coefficients generated in this work in Sec. II C.

profiles characteristic of the response of waxed porcine skin to 1070-nm laser exposure. A primary difference between this source data[7] and that used by Henriques[12,13,15] and Wu[34] is the nature of the heat deposition. The classic Moritz and Henriques study of thermal injury involved contact heating with hot liquid between 44 and 100 °C over durations between 1 s and 7 h.[15] Not only were some of these heating times very long, where both local and full body thermoregulatory responses begin to play a larger role, but the heat application was confined to the surface and only diffuses downward. The weakly absorbing, highly scattering nature of 1070-nm radiation in skin tissue resulted in more volumetric heat deposition, while the relatively smaller time scale may have prevented thermoregulation processes from biasing the results. Furthermore, and perhaps most relevantly, the damage criteria used by Moritz and Henriques was complete trans-epidermal necrosis,[15] which is representative of a greater burn degree than the MVL metric as defined in recent NIR laser skin damage studies.[6,7] The combination of these factors contributes to the modeled thresholds using the Henriques[12] and Wu[34] coefficients generally overestimating the required energy for a MVL when compared to the custom coefficients from this work and the experimental $ED_{50}$ values, as demonstrated by the absolute values in Tables IV–VII and the relative percent differences in Fig. 8.

### B. Prospective modeling

Given that the simulation framework presented in this paper has produced accurate results when retrospectively compared to experimental temperature profiles and $ED_{50}$ threshold data, we deployed the model prospectively for a series of single pulses in the nanosecond, microsecond, and millisecond time regimes, for beam diameters between 0.1 and 1 cm. There is minimal threshold data at these parameters in the literature, often because of the hardware limitations of available laser systems. Most solid state, continuous-wave systems do not switch faster than ~100 $\mu$s, and very few could output enough power under those conditions to produce skin damage, outside of a very small beam diameter.

Figure 9 displays the threshold prediction results for single-pulse, continuous-wave exposures with durations of 10 ns–10 s, at logarithmic decade intervals of time, for Gaussian $1/e^2$ beam diameters of 0.1, 0.3, 1, and 2 cm. The plot includes markers for the waxed $ED_{50}$ data from DeLisi *et al.*,[7] which is for durations of 0.01, 0.1, and 10 s at a beam diameter of ~1 cm. We also included the Q-switched single-pulse threshold from Rockwell and Goldman[4] for lightly pigmented human skin and our recent nanosecond-scale 1064-nm study[8] in shaved porcine skin. Both of these studies featured beam diameters of ~1 cm, though it was an approximate flattop in the case of Rockwell and Goldman[4] and a Gaussian $1/e^2$ diameter in the case of DeLisi *et al.*[7] The solid line represents the MPE limits, as defined by the ANSI Z136.1-2014 standard for 1070 nm laser exposures. This figure expresses the modeled thresholds and the experimental thresholds that feature a Gaussian beam in terms of peak radiant exposure calculated over the $1/e$ beam diameter, as this is standard practice when plotting them on the same graph as the MPE limits.

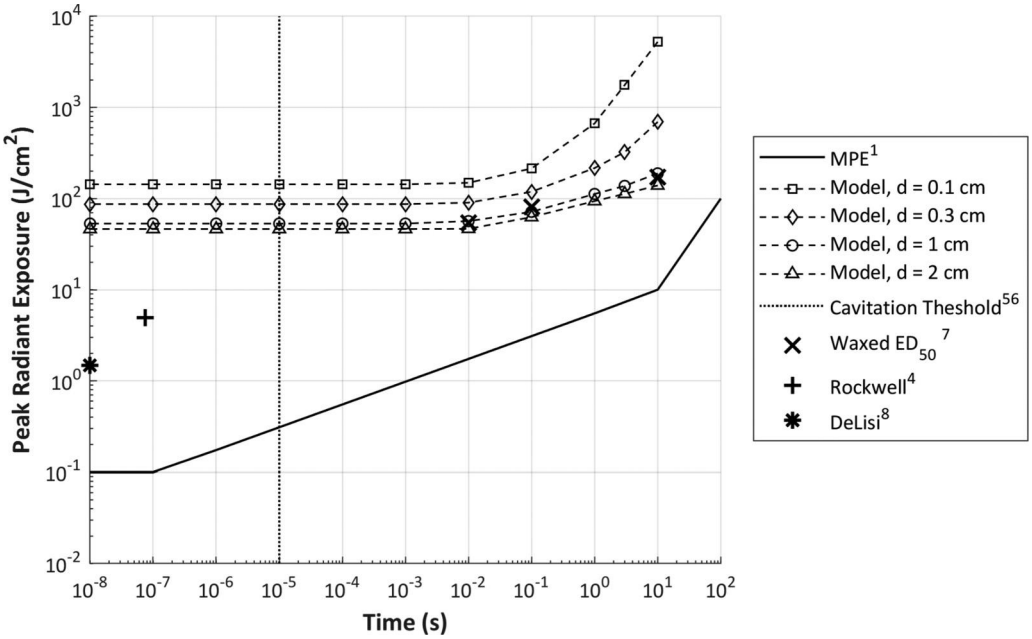


**FIG. 9.** Prospective modeling of thermal skin damage thresholds for single pulses ranging from 10 ns to 10 s, for beam diameters of 0.1, 0.3, 1, and 2 cm ($1/e^2$), along with select peak radiant exposure thresholds from the literature and the ANSI Z136.1-2014 MPE limits. Dashed lines are not fits and are only intended for visual aid. The model is assumed to not incorporate the photomechanical physics below the cavitation threshold.

The modeled thresholds in Fig. 9 feature similar behavior across exposure duration. For each beam diameter, the thermal damage radiant exposure threshold is essentially constant from the nanosecond region until ~10 ms, after which it then increases at a rate similar to the power function $y = ax^{-b}$, where $y$ is the radiant exposure and $x$ is exposure duration. This phenomenon is due to the absorption of energy by the tissue at a rate that exceeds the heat diffusion limit, as defined by the tissues thermal properties. Therefore, despite exponentially decreasing exposure durations, the same amplitude of threshold radiant exposure will result in nearly identical temperature rises that will not begin to significantly diffuse until several orders of magnitude later in time.

Figure 9 demonstrates that the modeled thresholds decrease as beam diameter increases, which correlates to a diminishing rate of radial thermal diffusion as the beam diameter approaches an infinite approximation (i.e., the 1D limit). The dependence of the damage threshold on beam diameter at short exposure durations is not unexpected. For exposure durations shorter than the thermal confinement time, heat cannot conduct out of the absorption volume while the laser is on, but the tissue temperature remains elevated long after the exposure and damage continues to accumulate during the cooling process. Thus, thermal conduction is relevant in determining the damage thresholds and results in beam diameter dependence. However, it is also possible that high scattering plays a significant role at this particular wavelength. Energy will be absorbed over a larger area in a high-scattering medium than in a low-scattering medium, resulting in a lower effective energy density in tissue compared to the energy density incident on the tissue. This requires a larger incident radiant exposure to generate the same absorbed radiant exposure in tissue, an effect that would be greater for smaller beams than for larger beams and thus drive beam diameter dependence of the thresholds. The role of scattering and thermal conduction on the spot size dependence of short duration damage thresholds should be investigated in more detail in the future.

Figure 10 provides a clear illustration of the effect of the thermal relaxation limitation for the 0.1 cm diameter case. Laser exposure thresholds up to 1–10 ms exhibit the same temperature rise, and although shorter exposures will reach that temperature orders of magnitude faster, they will not begin to cool until the millisecond time regime. This delay makes these short duration exposures look essentially the same to the Arrhenius integral since they all spend milliseconds at the same temperature, with negligible discrepancies in the nanosecond and microsecond range. However, once the exposure durations progress past the thermal relaxation limitation, the peak temperatures at the thresholds decreases as the exposure time increases, following the expected trend for tissue damage and protein denaturation studied by Henriques and Moritz.[13,15]

The discrepancy in Fig. 9 between the model predictions and the nanosecond-scale experimental thresholds[4,8] was not unexpected. The experimentally observed skin injuries at these points were most likely a result of photomechanical events such as melanin-mediated microcavitation and laser-induced breakdown as opposed to photothermal accumulation, as is common in the melanin-rich retina for short and ultrashort pulse laser systems.[54] Our model accounted for only the thermal diffusion physics for layered tissues and not the complex photomechanical

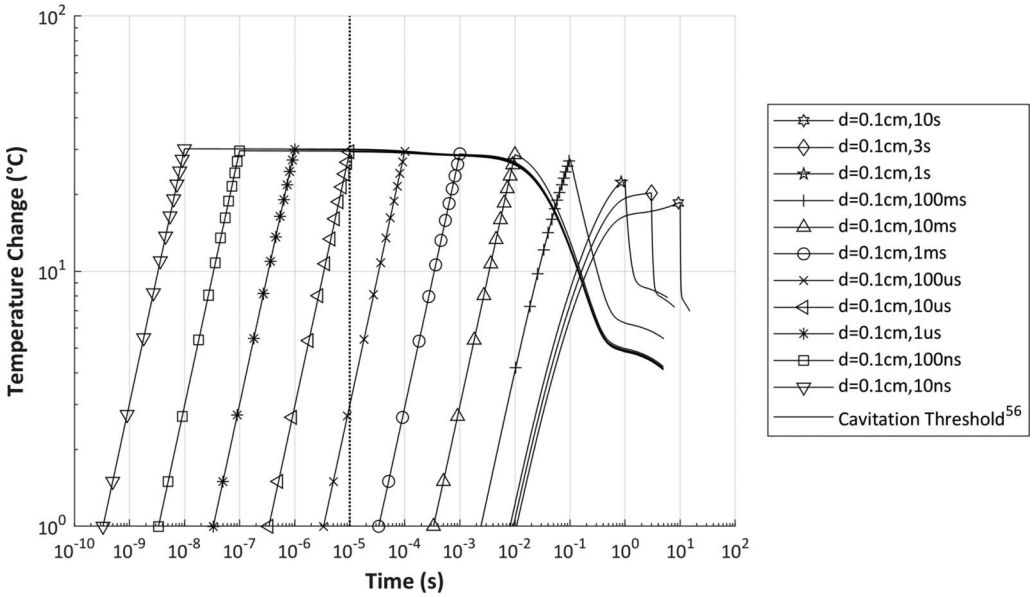


**FIG. 10.** Simulated temperature response for modeled threshold exposures with a Gaussian $1/e^2$ beam diameter of 0.1 cm for various logarithmically spaced exposure times. Shorter exposure duration plots include markers on the rise times, while longer durations only include markers at the peak for clarity. The cavitation threshold is marked by a vertical dotted line. The model is assumed to not incorporate the photomechanical physics below the cavitation threshold.

repercussions of cavitation bubble formation. Rockwell *et al.* determined that photomechanical damage is dominant for nanosecond-scale and shorter duration exposures.[54] Lee *et al.* concluded that melanin-mediated microcavitation and microbubble formation was the dominant damage mechanism in melanin-rich RPE cells for single pulses up to 10 $\mu$s,[55] while Brinkmann *et al.* reported similar observations for pulses up to 3 $\mu$s.[56] This modeling work demonstrated that upper-millisecond-scale and longer duration exposures are described quite well in purely photothermal terms. Figures 9 and 10 annotate the 10 $\mu$s microcavitation threshold by a vertical dotted line. We expect microcavitation to be the dominant injury mechanism for pulses shorter than 10 $\mu$s, and therefore the thermal model predictions are incorrect. However, we theorize that there is region in the microsecond-and lower-millisecond-scale of NIR laser exposure durations where both photothermal and photomechanical mechanisms intersect and interact. Exploring this region would require substantial development in laser technology, as systems with sufficient power to induce an MVL over a practical spot size (~1 cm) in 1–100 $\mu$s are not readily available. However, the prospective modeling capabilities provided by this work serve as a reasonable substitute for the photothermal component until eventual hardware advances allow for experimental validation, while further software development is necessary to integrate both photothermal and photomechanical processes in a unified multiphysics model of laser tissue exposure.

## CONCLUSION AND FUTURE WORK

This work presents a computational model of NIR laser photothermal response in lightly pigmented skin that demonstrated good temperature history matches with experimental data across a broad time range of exposure. We highlighted the importance of utilizing NIR optical properties that are consistent with the expected chromophore distribution in skin tissue, where melanin plays a critical role. Our derived value for epidermis optical absorption coefficient, along with the other material properties used, resulted in simulated temperature profiles that aligned with experimental thermography, unlike initial attempts that used epidermis optical properties from the literature. We employed a unique method of determining rate process coefficients for use in the Arrhenius integral based on experimental thermal profiles and demonstrated that values of $A = 2.74 \times 10^{94}$ 1/s and $E_a = 5.90 \times 10^5$ J/mol generate more accurate $ED_{50}$ threshold predictions than the rate process coefficients used in previous similar studies. The low percent differences between our modeled thresholds and the corresponding experimental thresholds provides confidence for employment of the model for prospective analysis.

The presence of hair follicles has a significant effect when comparing experimental and modeled damage thresholds, particularly for short pulses at high irradiances, due to their behavior as a local high-intensity heat source on the surface of the skin. Future computational modeling in this optical region can build upon our efforts by integrating high local absorption sources such as hair follicles. Furthermore, our finite-volume bioheat equation solution methodology serves as a comparison reference for more novel mathematical approaches to bioheat transfer such as Wharmby's fractional lumped capacitance model.[57] Additionally, given the relevance of melanin density on the epidermis optical absorption coefficient, this work suggests the need for sensitivity analysis of absorption coefficient and other parameter uncertainty given the expected variance of melanin distribution in the human population. As mentioned in the discussion, we can further investigate the relative contributions of thermal conduction and scattering to damage thresholds and beam diameter dependence for short pulses. Finally, this modeling framework can be leveraged prospectively to provide assessments of laser skin damage at other wavelengths and exposure conditions to validate or update the current MPE limits, particularly in regions where experimental data are unavailable.

## ACKNOWLEDGMENTS

Special thanks to Sebastian Liska and Byron Zollers at Nanohmics for their suggestions regarding modeling optimizations with the SESE software. Chad Oian at the Optical Radiation Bioeffects Branch of the Air Force Research Laboratory and Elharith Ahmed of SAIC provided some initial consultation on this project. Work contributed by SAIC was performed under USAF Contract Nos. FA8650-14-D-6519 and FA8650-19-C-6024. A portion of the initial results from this research was presented at the International Laser Safety Conference (ILSC) 2019 in Kissimmee, FL.[58] The opinions expressed on this document, electronic or otherwise, are solely those of the author(s). They do not represent an endorsement by or the views of the United States Air Force, the Department of Defense, or the United States Government.

## APPENDIX

This appendix describes the technique for determining rate process coefficients for use with the Arrhenius integral from input temperature profile data. We have generated a C++ library that implements this technique and made it publically available at https://github.com/CD3/libArrhenius.

### A. Introduction

Thermal damage to laser exposure is modeled as a first-order rate reaction in which the accumulation of damage, $\Omega$, is given by the Arrhenius integral

$$\Omega(t) = \int_0^t A e^{\frac{-E_a}{RT(t')}} dt', \tag{A1}$$

where $R$ is the universal gas constant and $T(t')$ is the tissue temperature as a function of time during the exposure. The coefficients $A$ and $E_a$ are the frequency factor and activation energy, respectively, and are often referred to collectively as the "Arrhenius coefficients." Most often, $\Omega = 1$ is defined to be the threshold for damage.

While the procedure for determining values for the Arrhenius coefficients from constant temperature exposures is well understood, determining values for $A$ and $E_a$ using the so-called "transient" thermal history (a time-varying temperature) measurements has long been a challenge. For a constant temperature exposure, Eq. (A1) becomes

$$\Omega(t) = A e^{\frac{-E_a}{RT}} t, \tag{A2}$$

where $T$ is the (constant) temperature during the exposure and $t$ is the time of exposure. At the threshold for damage, $\Omega = 1$, and this can be rearranged to give

$$\ln t = \frac{E_a}{R}\frac{1}{T} - \ln A. \tag{A3}$$

Estimates for $A$ and $E_a$ can be obtained by measuring the damage threshold temperature for various exposure times and performing a linear regression with Eq. (A3).

For transient temperature histories, Pearce *et al.* suggest first computing an "equivalent" constant temperature exposure for each transient temperature exposure and performing a linear regression with Eq. (A3) as normal.[36,59] Here, we detail a new method for estimating the Arrhenius coefficients from a set of transient temperature histories that are known to cause threshold damage.

### B. Relationship between $A$ and $E_a$

Consider a temperature history $T(t)$ that is known to cause threshold damage. For this case, the value of $\Omega$ is assumed to be 1, and we have

$$1 = \int_0^\tau A e^{\frac{-E_a}{RT(t)}} dt. \tag{A4}$$

The problem then is to determine the Arrhenius coefficients that make this true. For a single temperature history, Eq. (A4) does not define a unique combination of coefficients, but it does define a relationship between them. For any value of $E_a$, we can calculate the value of $A$ that satisfies Eq. (A4). Since $A$ is typically on the order of $10^{20}$–$10^{120}$, it will be more convenient to work with $\ln A$. We have

$$\ln A = LA = -\ln\left(\int_0^\tau e^{\frac{-E_a}{RT(t)}} dt\right), \tag{A5}$$

where we are using $LA$ to denote the natural log of $A$. We can, therefore, write $LA$ as a function of $E_a$. Pearce *et al.* used a cost function minimization to discover this relationship and noted that if one plots the values of $LA$ and $E_a$ that minimize the cost function, it looks like a straight line.[36,59] If we arrange Eq. (A3) to give

$$\ln A = \frac{1}{RT}E_a - \ln t, \tag{A6}$$

it shows a linear relationship between $LA$ and $E_a$ for constant temperature exposures, where the slope is given by $1/RT$ and the y-intercept is $\ln t$. Pearce *et al.* use this to compute an equivalent constant temperature exposure with temperature $T_{eq}$ and duration $t_{eq}$ by computing several pairs of ($LA$, $E_a$) that minimize their cost function and then fitting Eq. (B3) to these pairs.[36,59]

There are two things to note here. First, when $A$ is assumed to be independent of temperature, as is normally the case, then $LA$ for any value of $E_a$ can be directly computed by evaluating the integral in Eq. (A5) rather than cost function minimization, which is less expensive. Second, while $LA(E_a)$ does appear to be linear for transient temperature histories, Eq. (A6) only holds for constant temperature exposures. Plugging $E_a = 0$ into Eq. (A5) gives $LA = \ln t$ where $t$ is the integration time. A linear fit to that results in $LA \neq \ln t$ must diverge from the true $LA(E_a)$ for small $E_a$.

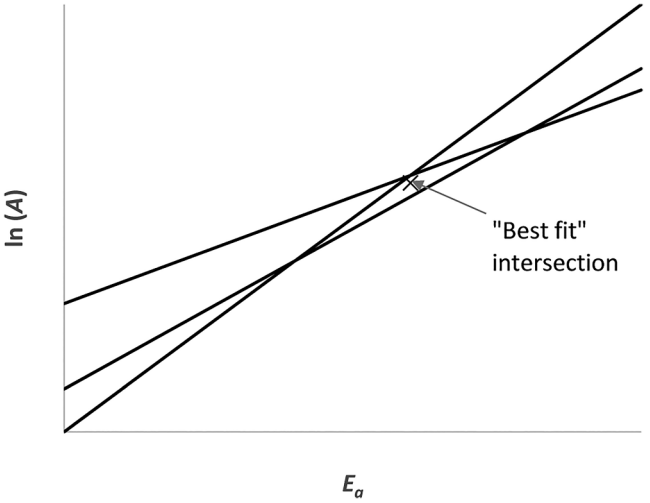


**FIG. 11.** An example of three lines that do not intersect at the same point. The "best fit" point of intersection is located at the value of $E_a$ ($x$ axis) that gives the smallest spread in ln ($A$) ($y$ axis).

To determine which pair of coefficients is the correct pair for a given system, multiple temperature histories are needed. For each temperature history, a function $LA_i(E_a)$ is computed using Eq. (A5), where $i$ denotes the function for the $i$th history. Ideally, all of these functions would intersect at the same point for a set of temperature histories known to cause threshold damage. In practice, this will not be the case and there are multiple points of intersection. Figure 11 illustrates this for three hypothetical temperature histories. The three lines in the figure intersect at three different positions, so it is not possible to identify a single set of coefficients as the true set. However, it is possible to determine a point of "best fit" intersection.

Our method is also based on minimizing a cost function, but our cost function differs from that used by Pearce *et al.*[36,59] We start with the assertion that the purpose of determining a set of coefficients is to allow for damage threshold predictions using the Arrhenius damage model. We wish to find a set of coefficients that result in the damage model predicting that each measured damage threshold temperature is very near the expected damage threshold.

### C. Damage thresholds and scaling thermal profiles

Consider a thermal profile generated by some sort of linear heating process in which the temperature rise caused by the heating scales linearly with the source term,

$$T(t) = T_0 + \alpha \Delta T(t). \tag{A7}$$

Here, $T_0$ is the baseline temperature before heating occurs, $\Delta T(t)$ is the time-dependent temperature rise, and $\alpha$ is the linear scaling

factor. While Pennes' bioheat equation is nonlinear due to the inclusion of blood perfusions, Clark *et al.* showed that including blood perfusion is important for modeling the temperature gradient in skin (i.e. predicting the correct surface temperature) before a laser exposure but not for modeling the temperature rise caused by the laser.[60] This means that, for a laser exposure, the heating can be considered linear and the parameter $\alpha$ will be directly proportional to the laser power/irradiance. Figure 7 shows a linear dependence between laser irradiance and the peak temperature recorded for this experiment, which indicates that the assumption of linearity is valid here.

The parameter $\alpha$ then can be used to define the "damage threshold scaling factor" for the temperature history, since plugging Eq. (A7) into Eq. (A4) gives

$$1 = \int_0^{\tau} A e^{\frac{-Ea}{R(T_0+\alpha\Delta T(t))}} dt. \tag{A8}$$

Given a set of coefficients, $A$ and $E_a$, and a temperature rise history $\Delta T(t)$, there is one value for $\alpha$ that will give $\Omega = 1$. This is the scaling factor required for the temperature history to cause threshold damage according to the damage model. In general, this parameter cannot be solved for analytically, but a numerical search can be used to determine the value of $\alpha$ that satisfies Eq. (A8).

If a temperature history is known to cause threshold damage, then $\alpha$ should equal one for that history. If multiple thermal profiles are known to cause threshold damage, then each should give $\alpha = 1$. We use this to measure the "goodness" of a set of coefficients based on our assertion that the purpose of the Arrhenius damage model is to calculate damage thresholds. The model should result in scaling factors for measured temperature histories at the damage threshold being very close to one.

Given $N$ temperature histories causing threshold damage, we calculate $\alpha$ for each and define the cost function to be

$$C = \sum_{i=1}^{N} (\alpha_i - 1)^2, \tag{A9}$$

where $\alpha_i$ is the calculated threshold for the $i$th profile. In principle, this cost function can be minimized with respect to $LA$ and $E_a$, since the $\alpha_i$s will depend on both. In practice, this is a computationally expensive task since a numerical search is required to compute each $\alpha_i$ for a given set of Arrhenius coefficients, which will require the Arrhenius integral to be evaluated multiple times. We have found that performing the minimization in two steps works well. First, search for the value of $E_a$ that gives the smallest variance in $LA$ values. Graphically, this is equivalent to looking for the value of $E_a$ where the lines in Fig. 11 are closest together. This can be done using a numerical minimization algorithm with the cost function for a given value of $E_a$ is defined as

$$C(E_a) = \sum_{i=1}^{N} (LA_i - \overline{LA})^2, \tag{A10}$$

where the bar over $LA$ denotes an average. This cost function only requires that the Arrhenius integral be evaluated $N$ times for one value of $E_a$. After selecting $E_a$, search for the value of $LA$ that minimizes the cost function defined in Eq. (A9).

### D. Comparison to other methods

Other methods for determining Arrhenius coefficients from transient thermal profiles have been suggested. Simanovskii *et al.* numerically integrated Eq. (A1) for multiple temperature histories $T(t)$ and noted that this should be the same for all damage threshold temperature histories.[61] They determined $E_a$ using a least squares method and then computed $A$ by some method that is not detailed. This is similar to our method, but differs in that we consider scaling factors for our cost function rather than the damage parameter.

The effective exposure method used by Pearce *et al.*[59] is perhaps more wide-spread as this is the method that was included in the 2011 updated version of Optical-Thermal Response of Laser-Irradiated Tissue.[36,59] Here, we compare the performance of our method to that of the effective exposure method by testing it on simulated data. First, we generated four temperature histories for exposure durations ranging from 5 ms to 5 s every decade. Then, we scaled each temperature history so that it would produce threshold damage ($\Omega = 1$) according to the Arrhenius damage model using the Welch–Polhamus[62] coefficients for damage to the retina ($A = 3.10 \times 10^{99}$ 1/s, $E_a = 6.28 \times 10^5$ J/mol). Finally, we fed these profiles into each method to compute values for $A$ and $E_a$. We did this for three different temperature history shapes: constant temperature, linear temperature rise, and simulated tissue exposure. Figure 12 shows the three different shapes for 0.5 s exposure.

Table IX lists the values obtained using our method compared to the effective exposure method. For the linear and simulated temperature histories, our method clearly performs better than the effective exposure method. Somewhat surprising is the constant

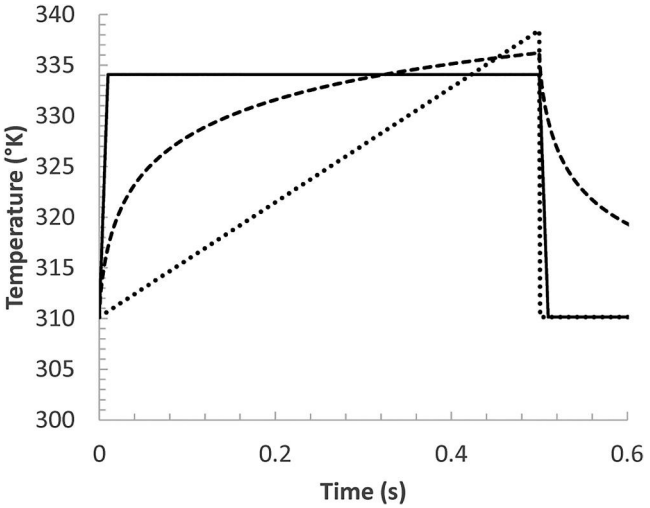


**FIG. 12.** Generated temperature profiles for a 0.5 s duration: constant temperature (solid line), linear temperature rise (dotted line), and simulated tissue exposure (dashed line).

**TABLE IX.** Comparison of each fitting method for various thermal profile shapes. The actual values used to generate each threshold thermal profile were $A = 3.10 \times 10^{99}\ s^{-1}$ and $E_a = 6.28 \times 10^5$ J/mol.

| Profile type | Method | Coefficient | Value |
|---|---|---|---|
| Constant temperature | Ours | $A$ | $7.84 \times 10^{100}\ s^{-1}$ |
| Constant temperature | Ours | $E_a$ | $6.37 \times 10^5$ J/mol |
| Constant temperature | Effective exposures | $A$ | $8.76 \times 10^{100}\ s^{-1}$ |
| Constant temperature | Effective exposures | $E_a$ | $6.38 \times 10^5$ J/mol |
| Linear temperature rise | Ours | $A$ | $3.10 \times 10^{99}\ s^{-1}$ |
| Linear temperature rise | Ours | $E_a$ | $6.28 \times 10^5$ J/mol |
| Linear temperature rise | Effective exposures | $A$ | $5.11 \times 10^{75}\ s^{-1}$ |
| Linear temperature rise | Effective exposures | $E_a$ | $4.82 \times 10^5$ J/mol |
| Simulated | Ours | $A$ | $3.09 \times 10^{99}\ s^{-1}$ |
| Simulated | Ours | $E_a$ | $6.28 \times 10^5$ J/mol |
| Simulated | Effective exposures | $A$ | $3.97 \times 10^{85}\ s^{-1}$ |
| Simulated | Effective exposures | $E_a$ | $5.46 \times 10^5$ J/mol |

temperature exposure results. Here, our method performs worst and the effective exposure method performs best, but the two perform very similarly.

## REFERENCES


[1]American National Standard Institute, "Z136.1 American National Standard for Safe Use of Lasers," in *ANSI Z136.1* (Laser Institute of America, Orlando, FL, 2014).

[2]C. P. Cain, G. D. Polhamus, W. P. Roach, D. J. Stolarski, K. J. Schuster, K. L. Stockton, B. A. Rockwell, B. Chen, and A. J. Welch, "Porcine skin visible lesion thresholds for near-infrared lasers including modeling at two pulse durations and spot sizes," J. Biomed. Opt. **11**, 041109 (2006).

[3]D. J. Finney and F. Tattersfield, *Probit Analysis* (Cambridge University Press, Cambridge, 1952).

[4]R. J. Rockwell, Jr., and L. Goldman, "Research on human skin laser damage thresholds," DTIC Report No. ADA012703 (Department of Dermatology and Laser Laboratories, University of Cincinnati, Cincinnati, OH, 1974).

[5]T. A. Eggleston, W. P. Roach, M. A. Mitchell, K. Smith, D. Oler, and T. E. Johnson, "Comparison of two porcine (*Sus scrofa domestica*) skin models for in vivo near-infrared laser exposure," Comp. Med. **50**, 391–397 (2000).

[6]R. Vincelette, G. D. Noojin, C. A. Harbert, K. J. Schuster, A. D. Shingledecker, D. J. Stolarski, S. S. Kumru, and J. W. Oliver, "Porcine skin damage thresholds for 0.6 to 9.5 cm beam diameters from 1070-nm continuous-wave infrared laser radiation," J. Biomed. Opt. **19**, 035007 (2014).

[7]M. P. DeLisi, M. S. Schmidt, A. F. Hoffman, A. M. Peterson, G. D. Noojin, A. D. Shingledecker, A. R. Boretsky, D. J. Stolarski, S. S. Kumru, and R. J. Thomas, "Thermal damage thresholds for multiple-pulse porcine skin laser exposures at 1070 nm," J. Biomed. Opt. **25**, 035001 (2019).

[8]M. P. DeLisi, A. M. Peterson, G. D. Noojin, A. D. Shingledecker, A. J. Tijerina, A. R. Boretsky, M. S. Schmidt, S. S. Kumru, and R. J. Thomas, "Porcine skin damage thresholds for pulsed nanosecond-scale laser exposure at 1064-nm," Proc. SPIE **10492**, 1049207 (2018).

[9]B. Chen, S. L. Thomsen, R. J. Thomas, and A. J. Welch, "Modeling thermal damage in skin from 2000-nm laser irradiation," J. Biomed. Opt. **11**, 064028 (2006).

[10]L. J. Irvin, P. D. Maseberg, G. D. Buffington, C. D. Clark, R. J. Thomas, M. L. Edwards, and J. Stolarski, "BTEC thermal model," DTIC Report No. ADA477371 (Air Force Research Laboratory, Optical Radiation Branch, San Antonio, TX, 2007).

[11]W. P. Roach, J. J. Thomas, K. J. Schuster, K. Stockton, D. J. Stolarski, M. S. Foltz, B. A. Rockwell, and C. P. Cain, "Model predictions and measured skin damage thresholds for 1.54-μm laser pulses in porcine skin," Proc. SPIE **4961**, 90–97 (2003).

[12]F. C. Henriques, Jr., "Studies of thermal injury: V. The predictability and the significance of thermally induced rate processes leading to irreversible epidermal injury," Arch. Pathol. **43**, 489–502 (1947).

[13]F. C. Henriques Jr. and A. R. Moritz, "Studies of thermal injury: I. The conduction of heat to and through skin and the temperatures attained therein. A theoretical and an experimental investigation," Am. J. Pathol. **23**, 530–549 (1947).

[14]A. R. Moritz, "Studies of thermal injury: III. The pathology and pathogenesis of cutaneous burns. An experimental study," Am. J. Pathol. **23**, 915–941 (1947).

[15]A. R. Moritz and F. C. Henriques, Jr., "Studies of thermal injury: II. The relative importance of time and surface temperature in the causation of cutaneous burns," Am. J. Pathol. **23**, 695–720 (1947).

[16]J. W. Oliver, R. Vincelette, G. D. Noojin, C. D. Clark, C. A. Harbert, K. J. Schuster, A. D. Shingledecker, S. S. Kumru, J. Maughan, and N. Kitzis, "Infrared skin damage thresholds from 1319-nm continuous-wave laser exposures," J. Biomed. Opt. **18**, 125002 (2013).

[17]J. W. Oliver, D. J. Stolarski, S. S. Kumru, C. P. Cain, C. J. Finkeldei, I. D. Noojin, R. J. Thomas, G. D. Buffington, G. D. Noojin, and H. M. Hodnett, "Infrared skin damage thresholds from 1940-nm continuous-wave laser exposures," J. Biomed. Opt. **15**, 065008 (2010).

[18]C. P. Cain, K. J. Schuster, J. J. Zohner, K. L. Stockton, D. J. Stolarski, R. J. Thomas, B. A. Rockwell, and W. P. Roach, "Visible lesion thresholds with pulse duration, spot size dependency, and model predictions for 1.54-μm, near-infrared laser pulses penetrating porcine skin," J. Biomed. Opt. **11**, 024001 (2006).

[19]J. J. Zohner, K. J. Schuster, L. J. Chavey, D. J. Stolarski, S. S. Kumru, B. A. Rockwell, R. J. Thomas, and C. P. Cain, "Visible lesion thresholds and model predictions for Q-switched 1318-nm and 1540-nm laser exposures to porcine skin," Proc. SPIE **6084**, 60840E (2006).

[20]B. Chen, S. L. Thomsen, R. J. Thomas, J. Oliver, and A. J. Welch, "Histological and modeling study of skin thermal injury to 2.0 μm laser irradiation," Lasers Surg. Med. **40**, 358–370 (2008).

[21]M. L. Denton, G. D. Noojin, M. S. Foltz, C. D. Clark, L. E. Estlack, B. A. Rockwell, and R. J. Thomas, "Spatially correlated microthermography maps threshold temperature in laser-induced damage," J. Biomed. Opt. **16**, 036003 (2011).

[22]M. L. Denton, E. M. Ahmed, G. D. Noojin, A. J. Tijerina, G. Gamboa, C. C. Gonzalez, and B. A. Rockwell, "Effect of ambient temperature and intracellular pigmentation on photothermal damage rate kinetics," J. Biomed. Opt. **24**, 065002 (2019).

[23]E. V. Salomatina, B. Jiang, J. Novak, and A. N. Yaroslavsky, "Optical properties of normal and cancerous human skin in the visible and near-infrared spectral range," J. Biomed. Opt. **11**, 064026 (2006).

[24]C. Mignon, D. J. Tobin, M. Zeitouny, and N. E. Uzunbajakava, "Shedding light on the variability of optical skin properties: Finding a path towards more accurate prediction of light propagation in human cutaneous compartments," Biomed. Opt. Express **9**, 852–872 (2018).
[25]A. N. Bashkatov, E. A. Genina, and V. V. Tuchin, "Optical properties of skin, subcutaneous, and muscle tissues: A review," J. Innovative Opt. Health Sci. **4**, 9–38 (2011).
[26]A. N. Bashkatov, E. A. Genina, V. I. Kochubey, and V. V. Tuchin, "Optical properties of human skin, subcutaneous and mucous tissues in the wavelength range from 400 to 2000nm," J. Phys. D: Appl. Phys. **38**, 2543–2555 (2005).
[27]T. L. Troy and S. N. Thennadil, "Optical properties of human skin in the near infrared wavelength range of 1000 to 2200 nm," J. Biomed. Opt. **6**, 167–176 (2001).
[28]Y. Du, X. H. Hu, M. Cariveau, X. Ma, G. W. Kalmus, and J. Q. Lu, "Optical properties of porcine skin dermis between 900 nm and 1500 nm," Phys. Med. Biol. **46**, 167–182 (2001).
[29]C. P. Cain, T. Milner, S. Telenkov, K. J. Schuster, K. L. Stockton, D. J. Stolarski, C. Condit, B. A. Rockwell, W. P. Roach, and A. J. Welch, "Porcine skin thermal response to near-IR lasers using a fast infrared camera," Proc. SPIE **5319**, 313–324 (2004).
[30]E. Zamora-Rojas, B. Aernouts, A. Garrido-Varo, W. Saeys, D. Pérez-Marín, and J. E. Guerrero-Ginel, "Optical properties of pig skin epidermis and dermis estimated with double integrating spheres measurements," Innovative Food Sci. Emerging Technol. **20**, 343–349 (2013).
[31]B. G. Zollars, G. J. Elpers, A. L. Goodwin, E. A. Early, N. J. Gamez, and R. J. Thomas, "Scalable effects simulation environment (SESE) Version 2.5.0," DTIC Report No. AD1082675 (Air Force Research Laboratory, San Antonio, TX, 2019).
[32]S. A. Prahl, "A Monte Carlo model of light propagation in tissue," Proc. SPIE **10305**, 1030509 (1989).
[33]C. Zhang, H. Lan, Y. Ye, and B. D. Estrade, "Parallel SOR iterative algorithms and performance evaluation on a Linux cluster," DTIC Report No. ADA449212 (Naval Research Laboratory, Stennis Space Center, Hancock, MS, 2005).
[34]Y. C. Wu, *A Modified Criterion for Predicting Thermal Injury* (National Bureau of Standards, Washington, DC, 1982).
[35]R. L. Palla, "A heat transfer analysis of scald injury," NBSIR Report No. 81-2320 (National Bureau of Standards, Washington, DC, 1981).
[36]S. Thomsen and J. A. Pearce, "Thermal damage and rate processes in biologic tissues," in *Optical-Thermal Response of Laser-Irradiated Tissue* (Springer, New York, 2010), pp. 487–549.
[37]L. D. Brown, D. Y. Kim, D. Brocksmith, M. Hodges, J. Liu, and G. F. Bouchard, "Characterization of normal skin thickness for various body regions, ages, and genders of yucatan miniature swine," Int. J. Toxicol. **30**, 101 (2011).
[38]G. Altshuler, M. Smirnov, and I. Yaroslavsky, "Lattice of optical islets: A novel treatment modality in photomedicine," J. Phys. D: Appl. Phys. **38**, 2732–2747 (2005).
[39]K. E. Spells, "The thermal conductivities of some biological fluids," Phys. Med. Biol. **5**, 139–154 (1960).
[40]A. N. Takata, L. Zaneveld, and W. Richter, "Laser-induced thermal damage of skin," DTIC Report No. ADA054612 (IIT Research Institute, Chicago, IL, 1977).
[41]T. E. Cooper and G. J. Trezek, "Correlation of thermal properties of some human tissue with water content," Aerosp. Med. **42**, 24–27 (1971).
[42]A. J. Welch, "The thermal response of laser irradiated tissue," IEEE J. Quantum Electron. **20**, 1471–1481 (1984).
[43]D. A. Torvi, "A finite element model of heat transfer in skin subjected to a flash fire," M.Sc. thesis, University of Alberta, 1992.
[44]J. Steketee, "Spectral emissivity of skin and pericardium," Phys. Med. Biol. **18**, 686–694 (1973).
[45]T. L. Bergman, F. P. Incropera, D. P. DeWitt, and A. S. Lavine, *Fundamentals of Heat and Mass Transfer* (Wiley, New York, 2011).
[46]F. Xu, T. J. Lu, K. A. Seffen, and E. Y. K. Ng, "Mathematical modeling of skin bioheat transfer," Appl. Mech. Rev. **62**, 050801 (2009).
[47]S. L. Jacques, see http://omlc.ogi.edu/news/jan98/skinoptics.html for Skin optics summary—Oregon Medical Laser Center News (1998).
[48]S. L. Jacques, "Optical properties of biological tissues: a review," Phys. Med. Biol. **58**, R37–R61 (2013).
[49]K. A. Sherwood, S. Murray, A. K. Kurban, and O. T. Tan, "Effect of wavelength on cutaneous pigment using pulsed irradiation," J. Invest. Dermatol. **92**, 717–720 (1989).
[50]R. Vincelette, A. Shingledecker, D. Roberson, K. E. Sheldon, J. Oliver, C. Washington, N. Jindra, R. W. Kornegay, and R. Figueroa, "A comparative study of melanin content and skin morphology for three commonly used laboratory swine (*Sus scrofa domestica*)," DTIC Report No. ADA576712 (Optical Radiation Bioeffects Branch, Air Force Research Laboratory, San Antonio, TX, 2012).
[51]W. Wagner and A. Pruß, "The IAPWS formulation 1995 for the thermodynamic properties of ordinary water substance for general and scientific use," J. Phys. Chem. Ref. Data **31**, 387–535 (2002).
[52]M. L. Huber, R. A. Perkins, D. G. Friend, J. V. Sengers, M. J. Assael, I. N. Metaxa, K. Miyagawa, R. Hellmann, and E. Vogel, "New international formulation for the thermal conductivity of $H_2O$," J. Phys. Chem. Ref. Data **41**, 033102 (2012).
[53]A. Roggan, K. Dorschel, O. Minet, D. Wolff, and G. Müller, "The optical properties of biological tissue in the near infrared wavelength range," in *Laser-Induced Interstitial Therapy* (SPIE Optical Engineering Press, Bellingham, WA, 1995), pp. 10–44.
[54]J. Zhou, J. K. Chen, and Y. Zhang, "Simulation of laser-induced thermotherapy using a dual-reciprocity boundary element model with dynamic tissue properties," IEEE Trans. Biomed. Eng. **57**, 238–245 (2010).
[55]B. A. Rockwell, R. J. Thomas, and A. Vogel, "Ultrashort laser pulse retinal damage mechanisms and their impact on thresholds," Med. Laser Appl. **25**, 84–92 (2010).
[56]H. Lee, C. Alt, C. M. Pitsillides, and C. P. Lin, "Optical detection of intracellular cavitation during selective laser targeting of the retinal pigment epithelium: dependence of cell death mechanism on pulse duration," J. Biomed. Opt. **12**, 064034 (2007).
[57]R. Brinkmann, G. Hüttmann, J. Rögener, J. Roider, R. Birngruber, and C. P. Lin, "Origin of retinal pigment epithelium cell damage by pulsed laser irradiance in the nanosecond to microsecond time regimen," Lasers Surg. Med. **27**, 451–464 (2000).
[58]A. W. Wharmby, "Fractional lumped capacitance," Fract. Calc. Appl. Anal. **21**, 1104–1119 (2018).
[59]M. P. DeLisi, N. J. Gamez, E. M. Ahmed, C. A. Oian, B. A. Rockwell, and R. J. Thomas, "Visible lesion threshold modeling of skin laser exposure at 1070-nm," Int. Laser Saf. Conf. **2019**, 111–118 (2019), paper no. 304.
[60]J. A. Pearce, K. Raghavan, and S. Thomsen, "Arrhenius model thermal damage coefficients for birefringence loss in rabbit myocardium," ASME Int. Mech. Eng. Congr. Expo. **37181**, 421–423 (2003).
[61]C. D. Clark III, R. J. Thomas, P. D. S. Maseberg, G. D. Buffington, L. J. Irvin, J. Stolarski, and B. A. Rockwell, "Modeling of surface thermodynamics and damage thresholds in the IR and THz regime," Proc. SPIE **6435**, 643505 (2007).
[62]D. M. Simanovskii, M. A. Mackanos, A. R. Irani, C. E. O'Connell-Rodwell, C. H. Contag, H. A. Schwettman, and D. V. Palanker, "Cellular tolerance to pulsed hyperthermia," Phys. Rev. E **74**, 011915 (2006).
[63]A. J. Welch and G. D. Polhamus, "Measurement and prediction of thermal injury in the retina of the rhesus monkey," IEEE Trans. Biomed. Eng. **31**, 633–644 (1984).